The *Enterprise*: A massive transposon carrying *Spok* meiotic drive genes

Aaron A. Vogan*[1], S. Lorena Ament-Velásquez[1], Eric Bastiaans[1,2], Ola Wallerman[3], Sven J. Saupe[4], Alexander Suh[1,5], Hanna Johannesson[1]

[1]Systematic Biology, Department of Organismal Biology, Uppsala University, Norbyvägen 18D, 752 36 Uppsala, Sweden
[2]Laboratory of Genetics, Wageningen University, Arboretumlaan 4, 6703 BD, Wageningen, The Netherlands
[3]Department of Medical Biochemistry and Microbiology, Comparative genetics and functional genomics; Uppsala University, Husargatan 3, 752 37 Uppsala, Sweden
[4]IBGC, UMR 5095, CNRS Université de Bordeaux, 1 rue Camille Saint Saëns, 33077 Bordeaux, cedex, France
[5]Present address: School of Biological Sciences, University of East Anglia, Norwich Research Park, NR4 7TU, Norwich, United Kingdom
*For Correspondence: aaron.vogan@ebc.uu.se

Abstract

The genomes of eukaryotes are full of parasitic sequences known as transposable elements (TEs). Most TEs studied to date are relatively small (50 – 12000 bp), but can contribute to very large proportions of genomes. Here we report the discovery of a giant tyrosine-recombinase-mobilized DNA transposon, *Enterprise*, from the model fungus *Podospora anserina*. Previously, we described a large genomic feature called the *Spok* block which is notable due to the presence of meiotic drive genes of the *Spok* gene family. The *Spok* block ranges from 110 kb to 247 kb and can be present in at least four different genomic locations within *P. anserina*, despite what is an otherwise highly conserved genome structure. We have determined that the reason for its varying positions is that the *Spok* block is not only capable of meiotic drive, but is also capable of transposition. More precisely, the *Spok* block represents a unique case where the *Enterprise* has captured the *Spok*s, thereby parasitizing a resident genomic parasite to become a genomic hyperparasite. Furthermore, we demonstrate that *Enterprise* (without the *Spoks*) is found in other fungal lineages, where it can be as large as 70 kb. Lastly, we provide experimental evidence that the *Spok* block is deleterious, with detrimental effects on spore production in strains which carry it. In contrast to the selfish role of the *Enterprise* in *P. anserina*, we hypothesize that the mobility of the *Enterprise* may also play an adaptive role in fungi when *Enterprise* undergoes horizontal transfer while carrying metabolic genes. This union of meiotic drivers and a transposon has created a selfish element of impressive size in *Podospora*, challenging our perception of how TEs influence genome evolution and broadening the horizons in terms of what the upper limit of transposition may be.

Introduction

Transposable elements (TEs) are major agents of change in eukaryotic genomes. Their ability to selfishly parasitise their host replication machinery has large impacts on both genome size and on gene regulation (Chénais et al. 2012). In extreme cases, TEs can contribute up to 85% of genomic content (Schnable et al. 2009) and expansion and reduction of TEs can result in rapid changes in both genome size and architecture (Haas et al. 2009; Talla et al. 2017; Möller and Stukenbrock 2017). Generally, TEs have small sizes (~50 – 12000 bp) and accomplish these large-scale changes through their sheer number. For example, there are ~1.1 million *Alu* elements in the human genome, which have had a large impact on genome evolution (Bennett et al. 2008; Jurka 2004). The largest known cases among Class I retrotransposons are long terminal repeat (LTR) elements that can be as large as 30 kb, but among Class II DNA transposons, Mavericks/Polintons are known to grow as large as 40 kb through the capture of additional open reading frames (ORFs) (Arkhipova and Yushenova 2019). Recently, a behemoth TE named *Teratorn* was described in teleost fish; it can be up to 182 kb in length, dwarfing all other known TEs. *Teratorn* has achieved this impressive size by fusing a *piggyBac* DNA transposon with a herpesvirus, thereby blurring the line between TEs and viruses (Inoue et al. 2017, 2018). Truly massive transposons may be lurking in the depths of many eukaryotic genomes, but the limitations of short-read genome sequencing technologies and the lack of population-level high-quality assemblies may make them difficult to identify.

The *Spok* block is a large genomic feature that was first identified thanks to the presence of the **spo**re **k**illing (*Spok*) genes in species from the genus *Podospora* (Vogan, Ament-Velásquez, et al. 2019; Grognet et al. 2014). The *Spoks* are selfish genetic elements that bias their transmission to the next generation in a process known as meiotic drive. Here, drive occurs by inducing the death of spores that do not inherit them, through a single protein that operates as both a toxin and an antidote (Vogan, Ament-Velásquez, et al. 2019; Grognet et al. 2014). The first *Spok* gene described, *Spok1*, was discovered in *P. comata* (Grognet et al. 2014). In *P. anserina*, the homologous gene *Spok2* is found at high population frequencies, while two other genes of the *Spok* family, *Spok3* and *Spok4,* are at low to intermediate frequencies (Vogan, Ament-Velásquez, et al. 2019). Unlike *Spok1* and *Spok2*, however, *Spok3* and *Spok4* are always associated with a large genomic region (the *Spok* block). The *Spok* block can be located at different chromosomal locations in different individuals, but is never found more than once in natural strains. The number of *Spok* genes and the location of the *Spok* block (which carries *Spok3*, *Spok4* or both) define the overall meiotic driver behavior of a given genome, which can be classified into the so-called ***P**odospora* **s**pore **k**illers or *Psk*s (Vogan, Ament-Velásquez, et al. 2019; van der Gaag et al. 2000). The *Spok* block stands out not only because of its size, typically around 150 kb, but also because there is otherwise high genome synteny among strains of *P. anserina* and with the related species *P. comata* and *P. pauciseta* (Vogan, Ament-Velásquez, et al. 2019).

The fact that the *Spok* block is found at unique genomic positions between otherwise highly similar strains is of prime interest as each novel *Spok* block position creates a unique meiotic drive type (*Psk*) due to the intricacies of meiosis in *Podospora*. In this study, we have determined that the reason the *Spok* block occurs at multiple genomic locations is that the *Spok* block itself is actually a unique version of the *Enterprise*, a novel DNA transposon that is mobilized by a tyrosine recombinase (YR). The *Spok* block represents an *Enterprise* that has captured meiotic drive genes and subsequently grown to a massive size through a gradual accumulation of DNA sequence. We find copies of *Enterprise* without meiotic drive genes in other fungal species that are at least 70 kb, placing *Enterprise* among the largest known TEs, even when not harbouring the *Spoks*. The *Spok* block version of *Enterprise* not only represents the largest TE discovered to date (reaching 247 kb), but is also capable of both transposition and meiotic drive. Furthermore, our data suggest that the *Spok* block is associated with fitness costs in *P. anserina*. This discovery drastically changes what we know about the size limits of transposition, and provides new insight into the role of massive TEs in eukaryotic genome evolution.

Results

Newly isolated *Podospora* strains reveal a novel spore killer type

We isolated and sequenced with Illumina HiSeq technology a strain of *P. anserina* (named Wa137) and two strains of *P. comata* (Wa131 and Wa139) collected in Wageningen, the Netherlands. The strains Wa137 and Wa139 were also sequenced using MinION Oxford Nanopore technology, achieving similar quality to published chromosome-level assemblies (**Supplementary Table 1**). Additionally, we included in our analyses all published long-read genomes of *P. anserina* (10 strains), *P. pauciseta* (one), and *P. comata* (one) (Espagne et al. 2008; Vogan, Ament-Velásquez, et al. 2019; Silar et al. 2019), which are mostly assembled at chromosome level, with respective genome sizes around 36 Mb (**Supplementary Table 1**). Previous work demonstrated that the *Spok* block can be found at three unique chromosomal positions among characterized *P. anserina* strains, defining the killer types *Psk-1*/*5* (with the *Spok* block located at chromosome 3), *Psk-2* (right arm of chromosome 5) and *Psk-7/8* (left arm of chromosome 5) (Vogan, Ament-Velásquez, et al. 2019) (**Table 1**). The newly isolated strain Wa137 was found to have a *Spok* block with the largest size yet reported (247 kb) and in a novel position (chromosome 1), conferring it a new spore killing phenotype that we named *Psk-9* (see Vogan, Ament-Velásquez, et al. (2019) for the principle of nomenclature). The published *P. pauciseta* genome has a *Spok* block in chromosome 4 (*Psk-P1*), but it seems to represent a fragmented version of the *P. anserina* blocks (Vogan, Ament-Velásquez, et al. 2019). Unlike *P. anserina* and *P. pauciseta*, the newly isolated strains of *P. comata* were found to have a single full-copy *Spok* gene (*Spok1*) which is not associated with any *Spok* block-like features, in agreement with the previously published reference genome of *P. comata* (**Table 1**) (Grognet et al. 2014; Silar et al. 2019).

The *Spok* block moves via transposition

A number of mechanisms exist by which a sequence can move within a genome, including reciprocal translocation, ectopic recombination, and transposition (Mieczkowski, Lemoine, and Petes 2006). We can rule out reciprocal translocations in the case of the *Spok* block, as overall chromosome synteny is preserved (Vogan, Ament-Velásquez, et al. 2019). Ectopic recombination is often mediated by TEs, and transposition is, by definition, the process of TE mobility. In order to determine a candidate mode by which the *Spok* block moves, we examined the four unique *Spok* block insertion sites. This analysis revealed that no specific TE was present at the insertion site, but showed that six base pairs (RGGTAG) are always present and are repeated at the end of the *Spok* block (**Figure 1A and B**). This repeated sequence may represent a target site duplication (TSD), which is a hallmark of transposition mechanisms (Wicker et al. 2007). Additionally, the *Psk-1* and *Psk-9 Spok* block insertion sites constitute a partially palindromic sequence ATACYT||AGGTAG (**Figure 1B**), a characteristic of some TE target sites (Linheiro and Bergman 2012). Together, this finding supports an explanation whereby the *Spok* block is mobilized like a TE via transposition.

The terminal sequences of TEs are often composed of structural features that are intrinsic to the transposition mechanism; LTRs for LTR retrotransposons and terminal inverted repeats (TIRs) for transposase-mobilized DNA transposons, for example (Wicker et al. 2007). These features can thus be used to determine the type of transposition or transposon underlying a given translocation. With this expectation, we examined the ends of the *Spok* block (which are very similar across all instances (Vogan, Ament-Velásquez, et al. 2019)), but found no such structural features. Curiously, the ends of the *Spok* block have been previously identified as two unclassified repetitive elements called *bufo* and *schoutedenella* (Espagne et al. 2008) (**Figure 1B**). We suspect that these unrelated elements actually represent the two ends of the *Spok* block (*bufo* representing the first 463 bp and *schoutedenella* representing the last 231 bp), and are found on their own in the genome as remains of previous, partially deleted, *Spok* block copies. To test this assumption, we mapped the location of all *bufo* and *schoutedenella* elements present in the *Podospora* genomes. We found that both elements can be identified throughout the chromosomes, with a tendency to locate in TE-rich areas in all species (**Figure 1C and Supplementary Figure 1**). In agreement with the postulate that the genomic copies of *bufo* and *schoutedenella* represent past *Spok* block insertions, at the *Psk-7* insertion site there is ~1200 bp of sequence that is homologous to the beginning of the *Spok* block. This is nearly 700 bp longer than what *bufo* alone represents, and further implies that the *Psk-7 Spok* block was inserted at the same site as a previous, now largely deleted copy. Together, these findings further support the idea that the *Spok* block inserts at the specific target site sequence RGGTAG which is duplicated during transposition (**Figure 1B**).

The *Spok* block accumulates sequence from the genome

As there were no structural features to guide us in our attempt to determine the mechanism through which the *Spok* block translocates, we examined the composition of the *Spok* block to

161 identify candidate genes capable of transposing it. We annotated all genome assemblies using
162 a modified version of the annotation pipeline in (Vogan, Ament-Velásquez, et al. 2019), relying
163 on additional RNA-seq data, as well as an improved, manually curated repeat library (see
164 Methods). The content of the different copies of the *Spok* block is largely overlapping (Vogan,
165 Lorena Ament-Velásquez, et al. 2019), although the Wa137 *Spok* block has a large region of
166 unique sequence resulting in a total size of 247 kb (**Figure 1C and Supplementary Figure 2**).
167 Very few genes were predicted within the *Spok* block by this methodology (as evidenced by the
168 dip in the orange track on the chr 1.2 scaffold; **Figure 1C**), so we manually annotated the *Spok*
169 block of representative strains (Wa53, Wa28, Wa58, and Wa137), which identified numerous
170 hypothetical protein-coding genes (e.g., 67 in the Wa137 *Spok block*), many of which appear to
171 be pseudogenes or gene fragments. The blocks do not generally exhibit unusually high TE load.
172 For example, the *Spok* block in Wa137 is only composed of 10.5% annotated TEs (compared to
173 genome wide estimates of 3 – 6%, **Supplementary Table S1**), nor do they appear to have a
174 strong signature of repeat-induced point mutation (RIP). RIP is a process that operates in
175 numerous fungi, including *Podospora* (Graïa et al. 2001), by specifically inducing C-to-T
176 mutations of any repeated sequence within the genome (Selker et al. 1987; Cambareri et al.
177 1989) and results in a drop of GC proportion in repetitive elements. Such a GC-drop is clear in
178 many regions of the *Podospora* genome, but is conspicuously absent within the *Spok* block
179 (Vogan, Ament-Velásquez, et al. 2019). While some of the predicted genes had identifiable
180 homologs within the *P. anserina* reference genome (orange features in **Figure 1C**), many are
181 absent from the reference but have sequence similarity to genes from other fungi (purple
182 features in **Figure 1C**). Of note, many of the predicted genes have potential roles in various
183 metabolic pathways, like metal tolerance or antimicrobial resistance (**Supplementary Table**
184 **S2**). It thus seems likely that the *Spok* block has grown to its large size, at least in part, by
185 accumulating non-repetitive sequence from elsewhere within the genome. The accumulation
186 does not appear to have been a single event, but was more likely many individual events, as the
187 genomic homologs are found on all chromosomes (green links in **Figure 1C**).

188 The *Enterprise*

189 The gene annotation provided us with very few clues as to the agent(s) responsible for the
190 translocation of the *Spok* block, so we turned to another approach. We hypothesize that the
191 *Spok* block was a much smaller element in the past, and that such an element could be still
192 transposing in the genomes of *Podospora* species. The closely related species *P. comata*
193 possesses both *bufo* and *schoutedenella* repeats, and appears to have large areas of homology
194 to the *Spok* block (**Supplementary Figure 1B**). We discovered that the *P. comata* strain Wa139
195 contains a 39 kb subtelomeric region on chromosome 5 (henceforth referred to as the
196 *Enterprise*) that is nearly completely composed of TEs and sequence homologous to the *Spok*
197 block (**Supplementary Figure 2**). The ends of the *Enterprise* are consistent with the *Spok* block
198 (both *bufo* and *schoutedenella* are present) and it possesses the RGGTAG target site
199 duplication (**Supplementary Figure 3A**). *Enterprise* is absent at the orthologous location in *P.*
200 *anserina* and *P. pauciseta*, is much smaller in the other *P. comata* strain T_D (5.5 kb), and
201 unassembled in Wa131. The other *P. comata* strains possess *bufo* and *schoutedenella* at this
202 location, suggesting that this specific *Enterprise* insertion is now polymorphic for its state of

203 degradation. However, it is difficult to fully recapitulate the history of the region due to the limited
204 number of strains and the fact that Wa139 also has another *schoutedenella* copy at the insertion
205 site that is absent in the other strains (**Supplementary Figure 3A**). Manual annotation revealed
206 five putative genes within the Wa139 *Enterprise*, four of which are homologous to the genes
207 within the *Spok* block and thus represent good candidates for involvement in the transposition of
208 *Enterprise* and therefore the *Spok* block.
209
210 None of these four genes have a known function and none are *Spok* homologs. We
211 examined their predicted protein domains, searched the *P. anserina* genomes for homologs,
212 and scanned genomic databases for similar sequences in an attempt to discern whether they
213 may be integral to the movement of the *Enterprise* (**Supplementary Table 3**). Only one of the
214 genes is a likely candidate for enacting the transposition of the *Enterprise*. This gene is always
215 present as the first ORF in the *Spok* block, but is degraded and interrupted by multiple TEs in
216 Wa139. The ORF possesses multiple domains which may be characteristic of specific
217 transposons, as determined by bioinformatic analysis (see Methods): a domain of unknown
218 function called DUF3435, a zinc finger domain, and a predicted CHROMO domain (**Figure 1D**).
219 Zinc finger domains are important for DNA binding, and CHROMO domains are implicated in
220 histone binding and may allow TEs to be targeted to specific regions of the genome (Kordis
221 2005). There is strong overlap between the DUF3435 domain and tyrosine recombinases (YRs),
222 a group of enzymes important for DNA integration of other selfish genetic elements known as
223 *Cryptons*, parasitic plasmids, and bacteria (Kojima and Jurka 2011). YRs are extremely
224 divergent, and there is little conserved sequence identity between this gene and known YRs, but
225 importantly, YRs are known to have a catalytic tetrad consisting of an R-H-R-Y motif (Esposito
226 and Scocca 1997), which is overlapping with the DUF3435 domain (**Figure 1D &**
227 **Supplementary Figure 4**). Given these results, we consider this gene to be a type of YR which
228 is responsible for transposing *Enterprise*, and name it "spore **ki**lling **r**elated **c**rypton" or *Kirc*.
229
230 From the evidence presented here, we propose that the *Spok* block and the homologous
231 region of Wa139 represent copies of a previously unknown group of DNA transposons, which
232 we name *Enterprise*. *Cryptons* are a type of DNA transposon defined only by the presence of a
233 YR domain (Wicker et al. 2007) and may possess a TSD or not (Kojima and Jurka 2011), thus
234 *Enterprise* can be classified as a novel group of *Crypton.* We define *Enterprise* as being
235 composed of a YR-encoding gene homologous to *Kirc*, and possessing a TSD (**Figure 1E**). The
236 *Spok* block therefore represents a specific version of *Enterprise* that contains *Spok* genes.
237
238 To confirm our hypothesis that *Enterprise* is capable of transposition and selfish
239 replication, we mined fungal genomes available on JGI MycoCosm for homologous proteins of
240 *Kirc* that are present in multiple copies within a single genome. We identified such a case in
241 *Melanconium sp.* NRRL 54901. In this genome, a homolog of *Kirc* is found at the beginning of a
242 ~70 kb region that is present in four copies in the genome. Critically, this region is flanked by the
243 same TSD as the *Spok* block and the target site is in its full palindromic context
244 CTACCT||AGGTAG (**Supplementary Figure 5**). The only gene homologous with the *Enterprise*
245 in *Podospora* is the *Kirc* homolog, thereby confirming that the minimal feature for transposition

246 is the putative YR-encoding gene, *Kirc,* and classifying this region of *Melanconium sp.* as an
247 *Enterprise.*

248 *Kirc* is wide-spread in filamentous fungi

249 Given the fact that *Enterprise* is present in at least one species outside of *Podospora*, we
250 queried GenBank with the sequence of *Kirc* using BLASTp to determine how widespread
251 *Enterprise* is. We recovered a total of 481 protein hits, which were almost exclusively from
252 within the Pezizomycotina, although putative homologs were identified from ten basidiomycete
253 genomes as well. A phylogeny of a representative set of sequences shows that the relationships
254 among the homologs do not follow the expected species phylogeny (**Figure 2**). Numerous
255 species have multiple *Kirc* homologs in the same genome, some of which are not closely
256 related. For example, within *P. anserina*, one homolog was recovered, Pa_5_10116 (see
257 Espagne et al. (2008) for *Podospora* gene notation), which appears to be distantly related to
258 *Kirc*, yet highly similar to homologs from *Fusarium*. Furthermore, Pa_5_10116 is pseudogenized
259 and absent in the close relatives of *P. anserina*, *P. comata* and *P. pauciseta*, consistent with it
260 being a transposable element. Attempts to describe TSDs in other fungi were largely
261 unsuccessful as conserved flanks could not be identified in most cases, which is not unusual for
262 *Cryptons* in general (Kojima and Jurka 2011). Thus, in the absence of additional evidence from
263 these fungal species, we consider these as *Enterprise*-like elements. Regardless, these results
264 suggest that *Enterprise* is a YR-mobilized group of DNA transposons that is spread throughout
265 fungal genomes.

266 The *Spok* block can be deleterious

267 In *P. anserina*, wild strains with more than one full copy of the *Spok* block have never been
268 found, although it is easy to generate them in the lab via crosses (Vogan, Ament-Velásquez, et
269 al. 2019). It is possible that the burden imposed by the *Spok* block on the host is quite high,
270 leading to selection to purge most copies in nature. To evaluate this hypothesis, we made use
271 of backcrosses of two of the *Psk* strains (Vogan, Ament-Velásquez, et al. 2019). The
272 backcrossed strains Psk1xS_{14} and Psk7xS_{14} are isogenic with the reference strain S, except that
273 S has no *Spok* block. Psk1xS_{14} has the *Spok* block on chromosome 3 and induces killing in 90%
274 of meioses, and Psk7xS_{14} has the *Spok* block on the left arm of chromosome 5 and induces
275 spore killing in 50% of meioses. We crossed strains either to themselves (no spore killing) or to
276 strain S (spore killing) and evaluated a number of traits related to fitness. Radial growth and
277 time to germination of spores produced by the matings showed no variation between crosses
278 (data not shown), however significant differences were observed among the amount of spores
279 produced by a cross (**Figure 3**). Specifically, crosses from selfings of Psk1xS_{14} produced
280 significantly fewer spores than from selfings of either S or Psk7xS_{14}, despite the fact that no
281 spore killing occurs, indicating that the *Psk-1 Spok* block inhibits spore production. This effect
282 was even greater in crosses between S and Psk1xS_{14}, and was most prominent when Psk1xS_{14}
283 was used as the female, suggesting a maternal effect. With both Psk1xS_{14} and Psk7xS_{14} more
284 spores were produced in the killing crosses than expected given the proportion of killing per
285 ascus (Vogan, Ament-Velásquez, et al. 2019). As there were no significant differences in the

286 amount of spores produced by Psk7xS_{14} than by S, this result suggests that the general
287 presence of the *Spok* block itself is not deleterious, but rather that the negative effect is due to
288 the specific content and/or to the genomic location of a given *Spok* block.

289 Discussion

290 Here we provide evidence that the *Spok* block is a variant of a newly described TE, *Enterprise*,
291 that moves throughout the genome of *P. anserina* by means of YR-mediated transposition. In
292 addition to this ability to move, the *Spok* block is also capable of meiotic drive due to the
293 presence of the *Spok* genes. Given the union of these two selfish properties, it can be asked
294 who is parasitizing whom. One possibility is that *Enterprise* has hijacked the *Spoks* in order to
295 increase its rate of transmission, thereby parasitizing a resident genomic parasite and becoming
296 a genomic hyperparasite. Support for this commandeering can be found in the distribution of the
297 *Spok* genes. In both *P. anserina* and *P. comata*, the *Spok* genes that are not found in
298 association with the *Spok* block are at high frequency (*Spok2* is found in 98% of strains isolated
299 in Wageningen (Vogan, Ament-Velásquez, et al. 2019), and so far *Spok1* has been found in all
300 analysed strains of *P. comata*). The *Spok* block is comparatively rare (~18% of strains from
301 Wageningen (Vogan, Ament-Velásquez, et al. 2019)), indicating that it may prevent the *Spoks*
302 from reaching high frequencies. Alternatively, the *Spok* genes may generally benefit from
303 moving throughout the genome. *Spok1* and *Spok2* are found at different locations in the
304 genome and are surrounded by TEs, suggesting they may have moved through other
305 mechanisms like TE-mediated ectopic recombination (Vogan, Ament-Velásquez, et al. 2019). It
306 may thus be advantageous for the *Spoks* to mobilize within TEs, like *Enterprise*, in order to
307 change their genomic position on a regular basis, due to the fact that this relocation will result in
308 a novel spore killing phenotype. Presumably, the population dynamics of meiotic drive ultimately
309 decide the fate of the *Spoks* (Nauta and Hoekstra 1993, Martinossi-Allibert, et al. 2020), but the
310 confederation of the *Spoks* and *Enterprise* as the *Spok* block may fundamentally change how
311 effective selection is at controlling either element.
312
313 Given that the results of the fitness experiments suggest that the *Spok* block can be
314 deleterious, there may be strong selection to purge any copies of *Enterprise*, but this may
315 ultimately be dependent on genomic context as insinuated by the differences in phenotypic
316 effect of carrying the *Psk-1* and *Psk-7 Spok* blocks. The *Psk-7 Spok* block is larger by nearly 50
317 kb, some of which includes known retrotransposons. Yet, only *Psk-1* showed a significant
318 decrease in the amount of spores produced. It thus seems probable that the location of the
319 block has a stronger deleterious effect rather than its content or size. The *Psk-1 Spok* block is
320 located close to the centromere on the left arm of chromosome 3. It is possible that the
321 increased amount of killing in *Psk-1* results in its poorer performance, although this cannot
322 explain the observed maternal effect. The rDNA cluster resides on the same chromosome arm
323 as the *Psk-1* block (Espagne et al. 2008). Given that this arm is only ~700 kb and the block itself
324 is 113 kb, the *Spok* block insertion might interfere with recombination, which is necessary for
325 proper segregation of rDNA (Tomson et al. 2006) and likely inhibits the ability of the strain to
326 produce viable spores. Moreover, the observation that there is not a large decrease in spore
327 production for *Psk-1* or *Pks-7* strains when involved in spore killing suggests that strains are

328 able to compensate for the lost spores in some way. This latter result has significant
329 implications to our understanding of spore killing as meiotic drive, as it shifts the system away
330 from providing the killer genotype a relative fitness advantage to an absolute fitness advantage
331 (Nauta and Hoekstra 1993; Lyttle 1991; Martinossi-Allibert et al. 2020). Explicitly, in the naïve
332 expectation, a spore killer that is 100% efficient would reduce the total amount of spores
333 produced in a killing cross to half. Thus, it does not produce more total offspring with its
334 genotype than a non-spore killing gene (relative advantage). However, if the strain carrying the
335 spore killer is able to compensate for the loss of spore production, and produce the same or
336 similar number of spores as in a non-killing cross (as observed here), the spore killer observes
337 an absolute advantage, as is the case for other types of meiotic drive, like female meiotic drive.
338 Therefore, spore killers may be more successful at invading and driving through populations
339 than previously thought.
340
341 The *Enterprise* clearly has the ability to move large amounts of genetic material around
342 the genome and TEs are known to be agents of horizontal gene transfer (HGT) (Schaack,
343 Gilbert, and Feschotte 2010; Gilbert and Feschotte 2018). As such, it is plausible that *Enterprise*
344 and related YR-mobilized DNA transposons may jump between species, and thereby transport
345 any additional genes they may carry. The phylogeny of the *Kirc* homologs is indicative of HGT
346 as it shows closely related *Kirc* homologs distributed amongst unrelated fungi. In at least two
347 cases, fungal TEs have been implicated as the vehicles for gene mobility of adaptive genes. In
348 the first case, a hAT element is associated with the HGT of toxin genes among cereal
349 pathogens (McDonald et al. 2019). The second case comes from a recent publication which
350 described a TE named *HEPHAESTUS* in the fungus *Paecilomyces* (Urquhart et al. 2020). It
351 carries multiple genes that provide resistance to at least five different heavy metals and shows
352 evidence of transfer with a distantly related species of *Penicillium*. In the latter example the TE
353 responsible for enacting the transposition is unidentified, but strikingly, a gene with a DUF3435
354 domain is present at the start of *HEPHAESTUS* (annotated as *hhpA*). We find little similarity
355 between *Kirc* and *hhpA* at the protein level, but our analyses here strongly suggest that *hhpA* is
356 also a YR and may be responsible for the reported transposition. Whether the *Enterprise* itself
357 can also play a role in adaptive HGT is unknown as of yet, but the potential certainly exists. We
358 note that most of the fungal genomes in which HGT has been reported (Wisecaver and Rokas
359 2015) possess genes containing DUF3435 domains, which together with the data from
360 *HEPHAESTUS* suggests a convergent role in this type of TE as a vector for HGT of adaptive
361 genes in fungi.

362 Conclusions

363 The constant ‘tug-of-war’ between TEs linking themselves to host genes, and the actions of
364 genome defense and selection to purge them is of key importance to the evolution of genome
365 architecture. It is likely that we are witnessing this fight play out to the extreme in *P. anserina*,
366 with the high effectiveness of both RIP and the *Spok* block, making *Podospora* an ideal system
367 in which to continue to study genomic conflict. The discovery that the up to 247 kb large *Spok*
368 block likely transposes through a YR-mediated mechanism moves the upper limit of TE size by
369 nearly 100 kb, and its hyper-selfishness combining TE mobility and meiotic drive adds a new

370 dynamic by which selfish elements exploit their host genome. This study not only changes our
371 perception of how TEs influence genome evolution, but also broadens the horizons in terms of
372 what may be possible through genetic manipulations in the laboratory. Understanding the
373 molecular mechanism of YR-mediated transposition should thus be of prime interest in future
374 research.
375
376

377 Methods

378

379 Fungal material

380
381 Strains used in this study were obtained from the Wageningen collection and cultivated as in
382 Vogan, Ament-Velásquez, et al. (2019). Strain S was used as the standard reference strain with
383 no *Spok* block. As spore killer strains for the fitness experiments (see below) we used the
384 backcrossed strains Psk1xS_{14} and Psk7xS_{14} (Vogan, Ament-Velásquez, et al. 2019), which
385 should be isogenic to S but with a *Spok* block in chromosome 3 and 5, respectively. The more
386 recently isolated strains Wa131, Wa137 and Wa139 were sampled during the fall of 2016
387 around Wageningen (the Netherlands) from dung of rabbit (Wa131 and Wa137, locality
388 Unksepad Oosterbeek) or horse (Wa139, locality Uiterwaarden Wolfswaard). Morphological
389 differences like smaller perithecia and abundant tomentose apricot-colored mycelium in HPM
390 medium (Vogan, Ament-Velásquez, et al. 2019), as well as analyses of sequence data, allowed
391 us to assign Wa131 and Wa139 to the species *P. comata*. Previously, only one strain from this
392 species, T_D, was known (Boucher, Nguyen, and Silar 2017; Vogan, Ament-Velásquez, et al.
393 2019), hence these new strains constitute a new report of this species for the Netherlands.
394

395 DNA and RNA extraction and sequencing

396 Following Vogan et al. (Vogan, Ament-Velásquez, et al. 2019), we grew monokaryotic strains on
397 PASM0.2 plates covered with a layer of cellophane. Genomic DNA for short-read sequencing
398 was extracted from 80-100 mg of fungal tissue with the Fungal/Bacterial Microprep kit (Zymo;
399 www.zymo.com). Paired-end libraries were prepared and sequenced using the Illumina HiSeq X
400 (150-bp-long) technology at the SNP and SEQ Technology platform (SciLifeLab, Uppsala,
401 Sweden). For RNA extraction, around 150 mg of harvested mycelium were frozen in liquid
402 nitrogen and stored at -80°C. We extracted total RNA from the grounded frozen tissue using the
403 RNeasy Plant Mini Kit (Qiagen, Hilden, Germany). Quality was checked on the agilent 2100
404 Bioanalyzer (Agilent Technologies, USA) and the RNA was treated with DNaseI (Thermo
405 Scientific). The sequencing library was prepared with a NEBNext Ultra Directional RNA Library
406 Prep Kit for Illumina (New England Biolabs). We purified polyA+ transcripts with the NEBNext

407 Poly(A) mRNA Magnetic Isolation Module (New England Biolabs). A paired-end library was
408 sequenced with Illumina HiSeq 2500 at the SNP and SEQ Technology platform.
409
410 For long-read sequencing, we grew the monokaryotic strains in PASM0.2 plates, from
411 where we sliced small agar cubes to inoculate liquid cultures of 200 ml 3% malt extract solution,
412 which were subsequently incubated in a shaker for 10-14 days at 27°C (Vogan, Ament-
413 Velásquez, et al. 2019). Mycelium aggregates were filtered from the flasks, any remaining agar
414 was removed, and around 1 g was stored at -20°C. As described in Sun et al. (2017), the tissue
415 was freeze-dried and macerated, followed by DNA extraction using Genomic Tip G-500
416 columns (Qiagen) and cleaning with the PowerClean DNA Clean-Up kit (MoBio Labs).
417 Additionally, DNA was purified using magnetic beads (Speed-Beads, GE) and eluted for 20 min
418 at 37°C followed by overnight storage at 4°C twice to increase concentration (around 65 ng/µl).
419 Wa137- was sequenced on an R9.5.1 Flowcell (Oxford Nanopore Technologies) with a modified
420 SQK-RAD004 protocol using 550 ng DNA to 1.5µl FRA to increase read lengths. Wa139- was
421 prepared using the ligation protocol (SQK-LSK109) and sequenced on an R9.4.1 flowcell.
422 Basecalling was done using Guppy v. 1.6.

423 Genome assembly

424 For most strains we used the assemblies produced in Vogan & Ament-Velásquez et al. (2019).
425 For newly sequenced strains, we produced new assemblies as follows. The adapters from the
426 Illumina HiSeq reads were identified with cutadapt v. 1.13 (Martin 2011) and removed using
427 Trimmomatic v. 0.36 (Bolger, Lohse, and Usadel 2014) using the following options:
428 ILLUMINACLIP:adapters.fasta:1:30:9 LEADING:20 TRAILING:20 SLIDINGWINDOW:4:20
429 MINLEN:30. Pairs with both forward and reverse reads after filtering were used for downstream
430 analyses. For the strain Wa131, which only has Illumina data, we used SPAdes v. 3.12.0
431 (Bankevich et al. 2012) with the k-mers 21,33,55,77 and the *--careful* option. For the strains
432 Wa137 and Wa139, the MinION reads with a mean Phred quality (QV) above 9 and longer than
433 1 kb were assembled using Minimap2 v. 2.11 and Miniasm v. 0.2 (Li 2018, 2016). The resulting
434 assembly was polished twice with Racon v. 1.3.1 (Vaser et al. 2017) using all MinION reads (no
435 filtering). Further polishing was done with the filtered Illumina reads in five consecutive rounds of
436 Pilon v. 1.22 (Walker et al. 2014). We used BWA v. 0.7.17 (Li and Durbin 2010) for short-read
437 mapping, with PCR duplicates marked using Picard v. 2.18.11
438 (http://broadinstitute.github.io/picard/), as well as local indel re-alignment using the Genome
439 Analysis Toolkit (GATK) v. 3.7 (Van der Auwera et al. 2013).
440
441 We assigned the scaffolds to chromosomes based on alignments to the reference
442 genome of the S strain (Espagne et al. 2008), available at the Joint Genome Institute
443 MycoCosm website (https://mycocosm.jgi.doe.gov/mycocosm/home) as “Podan2” (Grigoriev et
444 al. 2014). We discarded small contigs (<100kb) of rDNA repeats as well as mitochondrial-
445 derived sequences, except for the largest mitochondrial contig. We assessed the quality of the
446 final assemblies by visual inspection of the mapping of both long and short reads using
447 Minimap2 and BWA, respectively. Mean depth of coverage was calculated with QualiMap v.2.2

448 (Okonechnikov, Conesa, and García-Alcalde 2016). Other assembly statistics were calculated
449 with QUAST v. 4.6.3 (Mikheenko et al. 2016).

450 Genome annotation

451 A GitHub repository is available with Snakemake v. 5.4.4 (Köster and Rahmann 2012) pipelines
452 relevant to genome annotation at https://github.com/johannessonlab/SpokBlockPaper.
453
454 The TEs and other repeats in *P. anserina* were classified previously by Espagne et al.
455 (2008) based on the original reference genome of the S strain or "Podan1", and is hereafter
456 referred to as the "Espagne library". To explore the diversity of TEs in the newly generated
457 *Podospora* genomes, we identified repeats de novo and manually compared them to the
458 Espagne library to identify duplicates and new elements. Specifically, we ran RepeatModeler v.
459 1.0.8 (http://www.repeatmasker.org/RepeatModeler/) on the scaffolds larger than 50 kb of all
460 available long-read assemblies (Snakemake pipeline *PaTEs.smk*). Each resulting
461 RepeatModeler consensus was BLASTn-searched back to the original genome and the best 20
462 hits with 2-kb flanks were aligned with T-Coffee v. 12.00.7fb08c2 (Notredame, Higgins, and
463 Heringa 2000) (*TEManualCuration.smk*), and visually inspected for manual curation. The
464 curated consensuses were assigned to the Espagne et al. (2008) equivalents based on
465 similarity (allowing for RIP-induced mutations) or were given a new name when having no
466 homology to anything in the Espagne library. It was discovered that the *gypsy* element *crapaud*
467 has numerous diverged copies with unique LTRs. We annotated all *crapaud* LTRs that were in
468 multiple copies within *P. anserina* individually to improve repeat masking. We refer to the final
469 repeat library as "PodoTE-1.00" (available at the GitHub repository).
470
471 To generate a genome annotation of all assemblies, we ran an updated version of the
472 pipeline in Vogan & Ament-Velásquez et al. (2019), named *PaAnnotation.smk*. We used
473 MAKER v. 3.01.2 (Holt and Yandell 2011; Campbell et al. 2014) with the previously produced
474 training files used for the ab initio prediction programs GeneMark-ES v. 4.32 (Lomsadze et al.
475 2005; Ter-Hovhannisyan et al. 2008) and SNAP release 2013-06-16 (Lomsadze et al. 2005), as
476 well as the following dependencies: RepeatMasker v. 4.0.7 (http://www.repeatmasker.org/),
477 BLAST suite 2.6.0+ (Camacho et al. 2009), Exonerate v. 2.2.0 (Slater and Birney 2005), and
478 tRNAscan-SE v. 1.3.1 (Lowe and Eddy 1997). As evidence, we used STAR v. 2.6.1b (Dobin et
479 al. 2013) to produce transcript models (maximum intron length set to 1000 bp) of various RNA-
480 seq data sets. Specifically, we mapped the reads of the monokaryotic isolate Wa63- (*P.*
481 *anserina*) to the assembly PaWa63m (Vogan, Ament-Velásquez, et al. 2019), of the
482 monokaryotic isolate Wa131- (*P. comata*) to the assembly PcWa139m (this study), and of the
483 dikaryotic Psk7xS_{14} (*P. anserina*) to the assembly PaWa58m (Vogan, Ament-Velásquez, et al.
484 2019). We then processed the mapped reads with Cufflinks v. 2.2.1 (Trapnell et al. 2010) to
485 obtain the transcript models. As external evidence, we used CDS from the Podan2 annotation,
486 protein sequences from the T strain of *P. comata* (Silar et al. 2019), and a small dataset of
487 manually curated proteins. To aid in manual curation of selected regions (mostly the *Spok*
488 block), we visually inspected the mapping of RNA-seq reads of the different datasets, along with
489 CDS produced with TransDecoder v. 5.5.0 (Haas et al. 2013) on the Cufflinks models, as well

490 as the output of RepeatMasker ran externally from MAKER with the PodoTE-1.00 library.
491 Additionally, we queried predicted gene models into the NCBI databases (NCBI Resource
492 Coordinators 2016) to verify the annotations.
493
494 The *Kirc* protein sequence was analyzed with HHPred (Zimmermann et al. 2018) and
495 Gremlin (Balakrishnan et al. 2011). The Gremlin-generated alignment of *Kirc* homologs was
496 used to generate region-specific sequence logos with Weblogo (Crooks et al. 2004). The
497 relationship of *Kirc* to other YRs was confirmed by comparing the sequence to the crystal
498 structure of known YRs (CRE (PDB code 3mgv), XERD (1a0p), and FLP (1flo)) as well as the
499 protein sequence from the transposable element *Crypton-Cn1* using the software Promals3D
500 (Pei, Kim, and Grishin 2008).

501 Genome alignments

502 We used the NUCmer program from the MUMmer package v. 4.0.0beta2 (Kurtz et al. 2004)
503 using the parameters *-b 200 -c 22 --maxmatch* to align the *Spok* blocks to each other, and
504 *changed to -c 40* for whole-genome assemblies. To achieve higher sensitivity, we used BLASTn
505 from the BLAST suite 2.9.0 (Camacho et al. 2009) to search for the presence of the unclassified
506 repeats *bufo* and *schoutenella*. Both the NUCmer and the BLAST alignments were plotted using
507 Circos v. 0.69.6 (Krzywinski et al. 2009) along with manual curations of coding regions and
508 repetitive elements. The distribution of TE and gene content along chromosomes was
509 calculated in windows of 50 kb with steps of 10 kb using BEDtools v. 2.29.0 (Quinlan and Hall
510 2010; Quinlan 2014), with the utilities *makewindows* and *coverage*. The fraction of conservation
511 between blocks compared to the block in Wa137 was calculated by aligning the block
512 sequences (within the TSD) of Wa28 (*Psk-2*), Wa53 (*Psk-1*), Wa58 (*Psk-7*) and Wa139 with
513 NUCmer and the BEDtools utility *genomecov*. The Snakemake pipelines used to produce the
514 Circos plots (*CircosBlock.smk* and *CircosAllBlocks.smk*) are available at
515 https://github.com/johannessonlab/SpokBlockPaper.

516 Phylogenetic analyses

517 Homologs of *Kirc* were identified from GenBank using BLASTp with the truncated version of *Kirc*
518 from Wa53 that has no CHROMO domain. Nucleotide sequences of hits with e-values < 1e-100
519 were compiled along with a homolog from *P. anserina* (Pa_5_10116), and two homologs from
520 *Melanconium sp.* NRRL 54901 extracted from MycoCosm (see below), and aligned with
521 MACSE v. 2.03 (Ranwez et al. 2018). We used TrimAl v. 1.4.1 (Capella-Gutierrez, Silla-
522 Martinez, and Gabaldon 2009) to trim the resulting protein alignment with the *-gappyout* option.
523 We then used IQTree v. 1.6.8 (Kalyaanamoorthy et al. 2017; Nguyen et al. 2014) to produce a
524 Maximum Likelihood phylogeny with extended model selection (-m MFP). To estimate the
525 branch support, we produced 1000 standard bootstrap pseudoreplicates.
526
527 To search Mycocosm for other copies of *Enterprise* the following approach was taken.
528 The protein sequence of *Kirc* was used as a query with BLASTX against all genomes within
529 MycoCosm (as of February 2019). Genomes with multiple high confidence positive hits were

530 identified and the regions with putative *Kirc* homologs were manually extracted. Priority was
531 given to genomes where the hits were associated with large duplicated regions (>50 kb).
532 *Melanconium sp.* NRRL 54901 (produced as part of the 1KFG project; Spatafora et al. 2011)
533 had the most copies with clear termini.

534 Fitness assays

535 The cultures used for the crosses were revived from the -80 freezer on PASM0.2 (van
536 Diepeningen et al. 2008) at 27°C for several days and then stored at +4°C until use. Strains
537 were grown for 5 days on fresh PASM0.2 plates before inoculating the cross. In the crosses,
538 one strain was grown as mycelia and thereby assigned the female role, while a compatible
539 strain of the other mating type was assigned the male role by fertilizing the mycelia with
540 microconidia. The strain that was assigned the female role was grown in a 35 mm petri dish with
541 5 ml HPM medium (Vogan, Ament-Velásquez, et al. 2019) by inoculating a small cube of agar
542 with mycelium (~2 x 2 mm). In parallel, the strain that was assigned the male role was grown on
543 a 90 mm petri dish with micro conidiation medium (Esser 1974; King 2013) by inoculating seven
544 plugs of mycelium spread over the plate. After 7 days of growth, microconidia were harvested
545 by adding 5 ml of sterile water to the plate and sweep over the mycelium with a drigalski spatula
546 for 1 minute. The female mycelium was then fertilized with 0.5 ml of the microconidial
547 suspension. The suspension was carefully spread out to make sure all mycelium was covered.
548 The fertilized mycelia were then further incubated under standard conditions (27°C, 12/12
549 light/dark cycle) (Vogan, Ament-Velásquez, et al. 2019). The cultures were monitored daily for
550 signs of spores shot from the asci in order to score the first day of spore-shooting. To reduce
551 the complexity of the experiment, the strains used as female were always of mating type *mat+*.

552 At 6 days post-fertilization, single spores were collected with a needle to measure
553 germination frequency and growth speed. From each cross, 10 spores from 4-spored asci were
554 picked, and in cases with spore killing, an additional 10 spores from 2-spored asci were picked.
555 The 10 spores were transferred to a single 90 mm petri dish with PASM2 medium (van
556 Diepeningen et al. 2008) with 0.4% ammonium acetate added (to activate the spores) (Esser
557 1974; King 2013). Spores were spaced out in a predetermined pattern (4 lines of 2, 3, 3, 2
558 spores). After two days of incubation, the germination was scored and colony diameter was
559 measured in two directions. If there was no growth microscopic inspection was performed to
560 check whether a spore was present in the agar to avoid scoring no germination in case the
561 inoculation failed.

562 At 12 days post-fertilization, spores were harvested from the lids of each crossed culture
563 and used for estimating total spore yield. Spores were collected by pipetting 750 µl of harvest
564 liquid (1M NAOH, 0.025% SDS) in the lid. Spores were then scraped off the lid using the pipette
565 tip. The liquid was then collected into a 2 ml Eppendorf tube. Another 750 µl of harvest liquid
566 was used to repeat the process to make sure most of the spores were collected from the lid.
567 The tubes were then heated for 4 hours at 85°C, then shaken in a Qiagen Tissuelyser for 90
568 seconds at 30 Hz. After this, the tubes were stored at 4°C overnight. The cooled tubes were
569 again shaken in a Qiagen Tissuelyser for 90 seconds at 30 Hz. This process prevents the
570 clumping of spores. Total yield was determined by counting the amount of spores in a volume of

571 5 µl of 50x diluted suspension pipetted on an object glass using a stereomicroscope. Counts
572 were taken five times for each replicate cross. Statistical analyses were conducted in base R v.
573 3.5.0 to determine significance and power.

574 Acknowledgements

575 This work was supported by the European Research Council (ERC) grant ERC-2014-CoG
576 (project 648143, SpoKiGen) and The Swedish Research Council to H.J, and support from the
577 Lars Hierta Memorial Foundation and The Nilsson-Ehle Endowments of the Royal
578 Physiographic Society of Lund to S.L.A.V. We thank the support given by the National
579 Genomics Infrastructure (NGI) / Uppsala Genome center on massive parallel DNA sequencing.
580 The computations were performed on resources provided by SNIC through Uppsala
581 Multidisciplinary Center for Advanced Computational Science (UPPMAX) under the projects
582 SNIC 2017/1-567 and SNIC 2019/8-371. The sequence data of Melanconium sp. NRRL 54901
583 was produced by the US Department of Energy Joint Genome Institute http://www.jgi.doe.gov/
584 in collaboration with the user community. We would also like to thank Sergio Tusso and the TE
585 Jamboree of the Suh's Lab for useful advice.

586 References

587
588

589 Arkhipova, Irina R., and Irina A. Yushenova. 2019. "Giant Transposons in Eukaryotes: Is Bigger
590 Better?" *Genome Biology and Evolution* 11 (3): 906–18.
591 Balakrishnan S, Kamisetty H, Carbonell JG, Lee SI, Langmead CJ. 2011. Learning generative
592 models for protein fold families. *Proteins: Structure, Function, and Bioinformatics* 79: 1061–
593 1078.
594 Bankevich, Anton, Sergey Nurk, Dmitry Antipov, Alexey A. Gurevich, Mikhail Dvorkin, Alexander
595 S. Kulikov, Valery M. Lesin, et al. 2012. "SPAdes: A New Genome Assembly Algorithm and
596 Its Applications to Single-Cell Sequencing." *Journal of Computational Biology: A Journal of*
597 *Computational Molecular Cell Biology* 19 (5): 455–77.
598 Bennett, E. A., H. Keller, R. E. Mills, S. Schmidt, J. V. Moran, O. Weichenrieder, and S. E.
599 Devine. 2008. "Active *Alu* Retrotransposons in the Human Genome." *Genome Research* 18
600 (12): 1875-1883.
601 Bolger, Anthony M., Marc Lohse, and Bjoern Usadel. 2014. "Trimmomatic: A Flexible Trimmer
602 for Illumina Sequence Data." *Bioinformatics* 30 (15): 2114–20.
603 Boucher, Charlie, Tinh-Suong Nguyen, and Philippe Silar. 2017. "Species Delimitation in the
604 *Podospora anserina/P. pauciseta/P. comata* Species Complex (Sordariales)." *Cryptogamie,*
605 *Mycologie*. 38 (4): 485-506.
606 Camacho, Christiam, George Coulouris, Vahram Avagyan, Ning Ma, Jason Papadopoulos,
607 Kevin Bealer, and Thomas L. Madden. 2009. "BLAST+: Architecture and Applications."
608 *BMC Bioinformatics* 10: 421.
609 Cambareri, E., B. Jensen, E. Schabtach, and E. Selker. 1989. "Repeat-Induced G-C to A-T
610 Mutations in *Neurospora*." *Science*. 244 (4912): 1571-1575.
611 Campbell, Michael S., Carson Holt, Barry Moore, and Mark Yandell. 2014. "Genome Annotation
612 and Curation Using MAKER and MAKER-P." *Current Protocols in Bioinformatics* 48:

4.11.1–39.
Capella-Gutierrez, S., J. M. Silla-Martinez, and T. Gabaldon. 2009. “trimAl: A Tool for Automated Alignment Trimming in Large-Scale Phylogenetic Analyses.” *Bioinformatics* 25 (15): 1972-1973.
Chénais, Benoît, Aurore Caruso, Sophie Hiard, and Nathalie Casse. 2012. “The Impact of Transposable Elements on Eukaryotic Genomes: From Genome Size Increase to Genetic Adaptation to Stressful Environments.” *Gene* 509 (1): 7–15.
Crooks GE, Hon G, Chandonia JM, Brenner SE. 2004. WebLogo: a sequence logo generator. *Genome Research* 14: 1188–1190.
Diepeningen, Anne D. van, Alfons J. M. Debets, S. Marijke Slakhorst, and Rolf F. Hoekstra. 2008. “Mitochondrial pAL2-1 Plasmid Homologs Are Senescence Factors in *Podospora anserina* Independent of Intrinsic Senescence.” *Biotechnology Journal* 3 (6): 791–802.
Dobin, Alexander, Carrie A. Davis, Felix Schlesinger, Jorg Drenkow, Chris Zaleski, Sonali Jha, Philippe Batut, Mark Chaisson, and Thomas R. Gingeras. 2013. “STAR: Ultrafast Universal RNA-Seq Aligner.” *Bioinformatics* 29 (1): 15–21.
El-Gebali, Sara, Jaina Mistry, Alex Bateman, Sean R. Eddy, Aurélien Luciani, Simon C. Potter, Matloob Qureshi, et al. 2019. “The Pfam Protein Families Database in 2019.” *Nucleic Acids Research* 47 (D1): D427–32.
Espagne, Eric, Olivier Lespinet, Fabienne Malagnac, Corinne Da Silva, Olivier Jaillon, Betina M. Porcel, Arnaud Couloux, et al. 2008. “The Genome Sequence of the Model Ascomycete Fungus *Podospora anserina*.” *Genome Biology* 9 (5): R77.
Esposito, D., and J. J. Scocca. 1997. “The Integrase Family of Tyrosine Recombinases: Evolution of a Conserved Active Site Domain.” *Nucleic Acids Research* 25 (18): 3605–14.
Gaag, M. van der, A. J. Debets, J. Oosterhof, M. Slakhorst, J. A. Thijssen, and R. F. Hoekstra. 2000. “Spore-Killing Meiotic Drive Factors in a Natural Population of the Fungus *Podospora anserina*.” *Genetics* 156 (2): 593–605.
Gilbert, Clément, and Cédric Feschotte. 2018. “Horizontal Acquisition of Transposable Elements and Viral Sequences: Patterns and Consequences.” *Current Opinion in Genetics & Development* 49: 15–24.
Grigoriev IV, Nikitin R, Haridas S, Kuo A, Ohm R, Otillar R, Riley R, Salamov A, Zhao X, Korzeniewski F, Smirnova T, Nordberg H, Dubchak I, Shabalov I. (2014) “MycoCosm portal: gearing up for 1000 fungal genomes.” *Nucleic Acids Research* 42(1): D699-704.
Grognet, Pierre, Hervé Lalucque, Fabienne Malagnac, and Philippe Silar. 2014. “Genes That Bias Mendelian Segregation.” *PLoS Genetics* 10 (5): e1004387.
Haas, Brian J., Sophien Kamoun, Michael C. Zody, Rays H. Y. Jiang, Robert E. Handsaker, Liliana M. Cano, Manfred Grabherr, et al. 2009. “Genome Sequence and Analysis of the Irish Potato Famine Pathogen *Phytophthora infestans*.” *Nature* 461 (7262): 393–98.
Haas, Brian J., Alexie Papanicolaou, Moran Yassour, Manfred Grabherr, Philip D. Blood, Joshua Bowden, Matthew Brian Couger, et al. 2013. “De Novo Transcript Sequence Reconstruction from RNA-Seq Using the Trinity Platform for Reference Generation and Analysis.” *Nature Protocols* 8 (8): 1494–1512.
Holt, Carson, and Mark Yandell. 2011. “MAKER2: An Annotation Pipeline and Genome-Database Management Tool for Second-Generation Genome Projects.” *BMC Bioinformatics* 12 : 491.
Inoue, Yusuke, Masahiko Kumagai, Xianbo Zhang, Tomonori Saga, Deshou Wang, Akihiko Koga, and Hiroyuki Takeda. 2018. “Fusion of piggyBac-like Transposons and Herpesviruses Occurs Frequently in Teleosts.” *Zoological Letters* 4 (1): 6.
Inoue, Yusuke, Tomonori Saga, Takumi Aikawa, Masahiko Kumagai, Atsuko Shimada, Yasushi Kawaguchi, Kiyoshi Naruse, Shinichi Morishita, Akihiko Koga, and Hiroyuki Takeda. 2017. “Complete Fusion of a Transposon and Herpesvirus Created the *Teratorn* Mobile Element in Medaka Fish.” *Nature Communications* 8 (1): 551.

Jurka, Jerzy. 2004. “Evolutionary Impact of Human *Alu* Repetitive Elements.” *Current Opinion in Genetics & Development* 14 (6): 603–8.

Kalyaanamoorthy, Subha, Bui Quang Minh, Thomas K. F. Wong, Arndt von Haeseler, and Lars S. Jermiin. 2017. “ModelFinder: Fast Model Selection for Accurate Phylogenetic Estimates.” *Nature Methods* 14 (6): 587–89.

King, Robert C. 2013. *Handbook of Genetics: Volume 1 Bacteria, Bacteriophages, and Fungi*. Springer Science & Business Media.

Kojima, Kenji K., and Jerzy Jurka. 2011. “Crypton Transposons: Identification of New Diverse Families and Ancient Domestication Events.” *Mobile DNA* 2 (1): 12.

Kordis, Dusan. 2005. “A Genomic Perspective on the Chromodomain-Containing Retrotransposons: Chromoviruses.” *Gene* 347 (2): 161–73.

Köster, Johannes, and Sven Rahmann. 2012. “Snakemake – a Scalable Bioinformatics Workflow Engine.” *Bioinformatics* 28 (19): 2520–22.

Krzywinski, Martin, Jacqueline Schein, Inanç Birol, Joseph Connors, Randy Gascoyne, Doug Horsman, Steven J. Jones, and Marco A. Marra. 2009. “Circos: An Information Aesthetic for Comparative Genomics.” *Genome Research* 19 (9): 1639–45.

Kurtz, Stefan, Adam Phillippy, Arthur L. Delcher, Michael Smoot, Martin Shumway, Corina Antonescu, and Steven L. Salzberg. 2004. “Versatile and Open Software for Comparing Large Genomes.” *Genome Biology* 5 (2): R12.

Li, Heng. 2016. “Minimap and Miniasm: Fast Mapping and de Novo Assembly for Noisy Long Sequences.” *Bioinformatics* 32 (14): 2103–10.

———. 2018. “Minimap2: Pairwise Alignment for Nucleotide Sequences.” *Bioinformatics* 34 (18): 3094–3100.

Li, Heng, and Richard Durbin. 2010. “Fast and Accurate Long-Read Alignment with Burrows-Wheeler Transform.” *Bioinformatics* 26 (5): 589–95.

Linheiro, Raquel S., and Casey M. Bergman. 2012. “Whole Genome Resequencing Reveals Natural Target Site Preferences of Transposable Elements in *Drosophila melanogaster*.” *PloS One* 7 (2): e30008.

Lomsadze, Alexandre, Vardges Ter-Hovhannisyan, Yury O. Chernoff, and Mark Borodovsky. 2005. “Gene Identification in Novel Eukaryotic Genomes by Self-Training Algorithm.” *Nucleic Acids Research* 33 (20): 6494–6506.

Lowe, T. M., and S. R. Eddy. 1997. “tRNAscan-SE: A Program for Improved Detection of Transfer RNA Genes in Genomic Sequence.” *Nucleic Acids Research* 25 (5): 955–64.

Lyttle, T. W. 1991. “Segregation Distorters.” *Annual Review of Genetics* 25: 511–57.

Martin, Marcel. 2011. “Cutadapt Removes Adapter Sequences from High-Throughput Sequencing Reads.” *EMBnet.journal*. 17 (1): 10-12.

Ivain Martinossi-Allibert, Carl Veller, S. Lorena Ament-Velásquez, Aaron A. Vogan, Claus Rueffler, Hanna Johannesson. 2020. “Invasion and maintenance of spore killing in ascomycete fungi.” *bioRxiv* 2020.04.06.026989.

McDonald, Megan C., Adam P. Taranto, Erin Hill, Benjamin Schwessinger, Zhaohui Liu, Steven Simpfendorfer, Andrew Milgate, and Peter S. Solomon. 2019. “Transposon-Mediated Horizontal Transfer of the Host-Specific Virulence Protein *ToxA* between Three Fungal Wheat Pathogens.” *mBio* 10 (5): e01515-19.

Mieczkowski, Piotr A., Francene J. Lemoine, and Thomas D. Petes. 2006. “Recombination between Retrotransposons as a Source of Chromosome Rearrangements in the Yeast *Saccharomyces cerevisiae*.” *DNA Repair* 5 (9-10): 1010–20.

Mikheenko, Alla, Gleb Valin, Andrey Prjibelski, Vladislav Saveliev, and Alexey Gurevich. 2016. “Icarus: Visualizer for de Novo Assembly Evaluation.” *Bioinformatics* 32 (21): 3321–23.

Möller, Mareike, and Eva H. Stukenbrock. 2017. “Evolution and Genome Architecture in Fungal Plant Pathogens.” *Nature Reviews. Microbiology* 15 (12): 771.

Nauta, M. J., and R. F. Hoekstra. 1993. “Evolutionary Dynamics of Spore Killers.” *Genetics* 135

(3): 923–30.
NCBI Resource Coordinators. 2016. “Database Resources of the National Center for Biotechnology Information.” *Nucleic Acids Research* 44 (D1): D7–19.
Nguyen, Lam-Tung, Heiko A. Schmidt, Arndt von Haeseler, and Bui Quang Minh. 2014. “IQ-TREE: A Fast and Effective Stochastic Algorithm for Estimating Maximum-Likelihood Phylogenies.” *Molecular Biology and Evolution* 32 (1): 268–74.
Notredame, C., D. G. Higgins, and J. Heringa. 2000. “T-Coffee: A Novel Method for Fast and Accurate Multiple Sequence Alignment.” *Journal of Molecular Biology* 302 (1): 205–17.
Okonechnikov, Konstantin, Ana Conesa, and Fernando García-Alcalde. 2016. “Qualimap 2: Advanced Multi-Sample Quality Control for High-Throughput Sequencing Data.” *Bioinformatics* 32 (2): 292–94.
Pei, Jimin, Bong-Hyun Kim, and Nick V. Grishin. 2008. “PROMALS3D: A Tool for Multiple Protein Sequence and Structure Alignments.” *Nucleic Acids Research* 36 (7): 2295–2300.
Quinlan, Aaron R. 2014. “BEDTools: The Swiss-Army Tool for Genome Feature Analysis.” *Current Protocols in Bioinformatics* 47: 11.12.1–34.
Quinlan, Aaron R., and Ira M. Hall. 2010. “BEDTools: A Flexible Suite of Utilities for Comparing Genomic Features.” *Bioinformatics* 26 (6): 841–42.
Ranwez, Vincent, Emmanuel J. P. Douzery, Cédric Cambon, Nathalie Chantret, and Frédéric Delsuc. 2018. “MACSE v2: Toolkit for the Alignment of Coding Sequences Accounting for Frameshifts and Stop Codons.” *Molecular Biology and Evolution* 35 (10): 2582–84.
Schaack, Sarah, Clément Gilbert, and Cédric Feschotte. 2010. “Promiscuous DNA: Horizontal Transfer of Transposable Elements and Why It Matters for Eukaryotic Evolution.” *Trends in Ecology & Evolution* 25 (9): 537–46.
Schnable, Patrick S., Doreen Ware, Robert S. Fulton, Joshua C. Stein, Fusheng Wei, Shiran Pasternak, Chengzhi Liang, et al. 2009. “The B73 Maize Genome: Complexity, Diversity, and Dynamics.” *Science* 326 (5956): 1112–15.
Selker, E. U., E. B. Cambareri, B. C. Jensen, and K. R. Haack. 1987. “Rearrangement of Duplicated DNA in Specialized Cells of *Neurospora*.” *Cell* 51 (5): 741–52.
Silar, Philippe, Jean-Marc Dauget, Valérie Gautier, Pierre Grognet, Michelle Chablat, Sylvie Hermann-Le Denmat, Arnaud Couloux, Patrick Wincker, and Robert Debuchy. 2019. “A Gene Graveyard in the Genome of the Fungus *Podospora comata*.” *Molecular Genetics and Genomics: MGG* 294 (1): 177–90.
Slater, Guy St C., and Ewan Birney. 2005. “Automated Generation of Heuristics for Biological Sequence Comparison.” *BMC Bioinformatics* 6: 31.
Spatafora, Joey. 2011. “1000 fungal genomes to be sequenced.” *IMA Fungus* 2 (2): 41-45.
Sun, Yu, Jesper Svedberg, Markus Hiltunen, Pádraic Corcoran, and Hanna Johannesson. 2017. “Large-Scale Suppression of Recombination Predates Genomic Rearrangements in *Neurospora tetrasperma*.” *Nature Communications* 8 (1): 1140.
Talla, Venkat, Alexander Suh, Faheema Kalsoom, Vlad Dincă, Roger Vila, Magne Friberg, Christer Wiklund, and Niclas Backström. 2017. “Rapid Increase in Genome Size as a Consequence of Transposable Element Hyperactivity in Wood-White (*Leptidea*) Butterflies.” *Genome Biology and Evolution* 9 (10): 2491–2505.
Ter-Hovhannisyan, V., A. Lomsadze, Y. O. Chernoff, and M. Borodovsky. 2008. “Gene Prediction in Novel Fungal Genomes Using an Ab Initio Algorithm with Unsupervised Training.” *Genome Research* 18 (12) 1979-1990.
Tomson, Brett N., Damien D’Amours, Brittany S. Adamson, Luis Aragon, and Angelika Amon. 2006. “Ribosomal DNA Transcription-Dependent Processes Interfere with Chromosome Segregation.” *Molecular and Cellular Biology* 26 (16): 6239–47.
Trapnell, Cole, Brian A. Williams, Geo Pertea, Ali Mortazavi, Gordon Kwan, Marijke J. van Baren, Steven L. Salzberg, Barbara J. Wold, and Lior Pachter. 2010. “Transcript Assembly and Quantification by RNA-Seq Reveals Unannotated Transcripts and Isoform Switching

during Cell Differentiation." *Nature Biotechnology* 28 (5): 511–15.

Urquhart, A. S., Chong, N. F., Yang, Y., & Idnurm, A. (2020). "Eukaryotic transposable elements as "cargo carriers": the forging of metal resistance in the fungus *Paecilomyces variotii*." *bioRxiv* 2020.03.06.981548.

Van der Auwera, Geraldine A., Mauricio O. Carneiro, Chris Hartl, Ryan Poplin, Guillermo Del Angel, Ami Levy-Moonshine, Tadeusz Jordan, et al. 2013. "From FastQ Data to High Confidence Variant Calls: The Genome Analysis Toolkit Best Practices Pipeline." *Current Protocols in Bioinformatics* 43: 11.10.1–33.

Vaser, Robert, Ivan Sović, Niranjan Nagarajan, and Mile Šikić. 2017. "Fast and Accurate de Novo Genome Assembly from Long Uncorrected Reads." *Genome Research* 27 (5): 737–46.

Vogan, Aaron A., S. Lorena Ament-Velásquez, Alexandra Granger-Farbos, Jesper Svedberg, Eric Bastiaans, Alfons J. M. Debets, Virginie Coustou, et al. 2019. "Combinations of *Spok* Genes Create Multiple Meiotic Drivers in *Podospora*." *eLife* 8: e46454.

Walker, Bruce J., Thomas Abeel, Terrance Shea, Margaret Priest, Amr Abouelliel, Sharadha Sakthikumar, Christina A. Cuomo, et al. 2014. "Pilon: An Integrated Tool for Comprehensive Microbial Variant Detection and Genome Assembly Improvement." *PloS One* 9 (11): e112963.

Wicker, Thomas, François Sabot, Aurélie Hua-Van, Jeffrey L. Bennetzen, Pierre Capy, Boulos Chalhoub, Andrew Flavell, et al. 2007. "A Unified Classification System for Eukaryotic Transposable Elements." *Nature Reviews. Genetics* 8 (12): 973–82.

Wisecaver, Jennifer H., and Antonis Rokas. 2015. "Fungal Metabolic Gene Clusters-Caravans Traveling across Genomes and Environments." *Frontiers in Microbiology* 6: 161.

Zimmermann L, Stephens A, Nam SZ, Rau D, Kübler J, Lozajic M, Gabler F, Söding J, Lupas AN, Alva V. 2018. A completely reimplemented MPI bioinformatics toolkit with a new HHpred server at its core. *Journal of Molecular Biology* 430: 2237–2243.

Figures

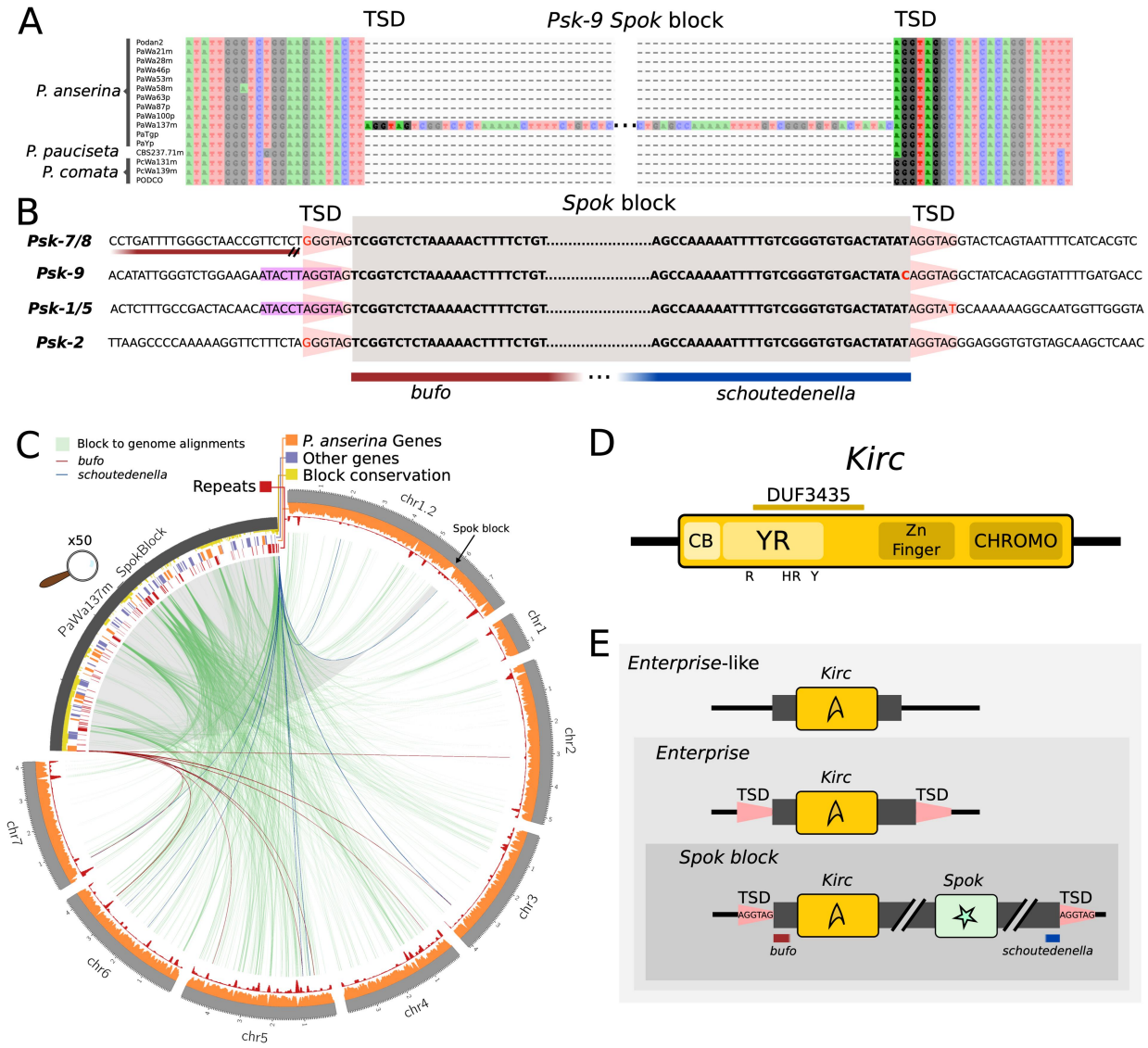

Figure 1. The genomic context of the *Spok* Block. **A** An alignment of the region where the *Spok* block is located in the strain Wa137 (*Psk*-9) from all *P. anserina* genomes. Putative target site duplication (TSD) is highlighted. Only the ends of the *Spok* block are shown for clarity. **B** An alignment of the ends of four versions of the *Spok* block displaying the TSD (pink trapezoid). The flanks of the *Spok* block that relate to the unclassified repeats *bufo* and *schoutedenella* are underlined in red and blue, respectively. Note that for *Psk-7*, the *Spok* block is inserted immediately next to a truncated *bufo* element. **C** A Circos plot of the genome of Wa137 (light grey track, size in Mb) aligned against its own *Spok* block (dark grey, enlarged by 50x). The tracks on the *Spok* block from outside inward represent: the conservation of regions among the different iterations of the *Spok* block where the height of the conservation track is equivalent to

804 the number of blocks that have a given position (yellow); gene models from manual annotation
805 of the *Spok* block, where genes with homologs within the reference genome of *P. anserina* are
806 marked in orange and those without homologs are marked in purple; and annotated repeated
807 elements (red). The tracks on the chromosomal scaffolds show the coverage of genic regions
808 (orange) and repeats (red) calculated in sliding windows of 50 kb with steps of 10 kb. Green
809 lines connect homologous segments based on MUMmer alignments. The unclassified repetitive
810 elements *bufo* and *schoutedenella* are connected in dark red and blue segments, respectively,
811 based on BLASTn searches. **D** Cartoon representation of the predicted protein for the ORF *Kirc*
812 with domains predicted by bioinformatics analyes. The catalytic tetrad is marked below the
813 protein model. **E** Cartoon model of the hierarchical nomenclature of *Enterprise*-like elements,
814 *Enterprise* and the *Spok* block. See Supplementary Figure 3 for more detailed depictions of the
815 *Spok* block.

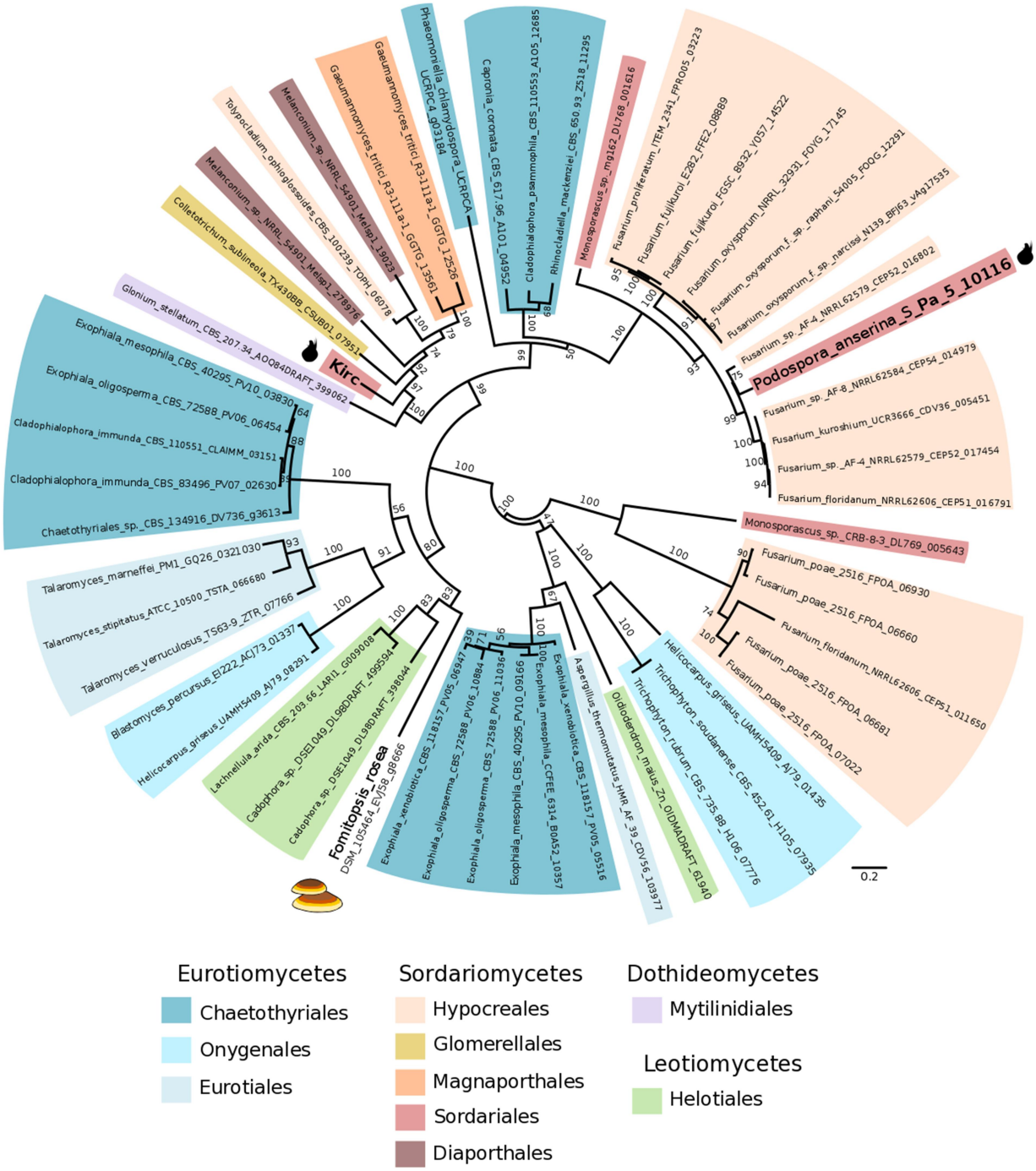

Figure 2. Unrooted Maximum likelihood phylogenetic tree showing the relationship between *Kirc* and other homologs from fungi. Bootstrap support values are shown above branches. Branch lengths are proportional to the scale bar (amino acid substitution per site). Taxonomic rank is indicated with coloured highlights. The sequences present in *Podospora anserina* and in the basidiomycete *Fomitopsis rosea* are marked with cartoons of the corresponding fruiting bodies. Nomenclature is formatted as species_strain_protein code.

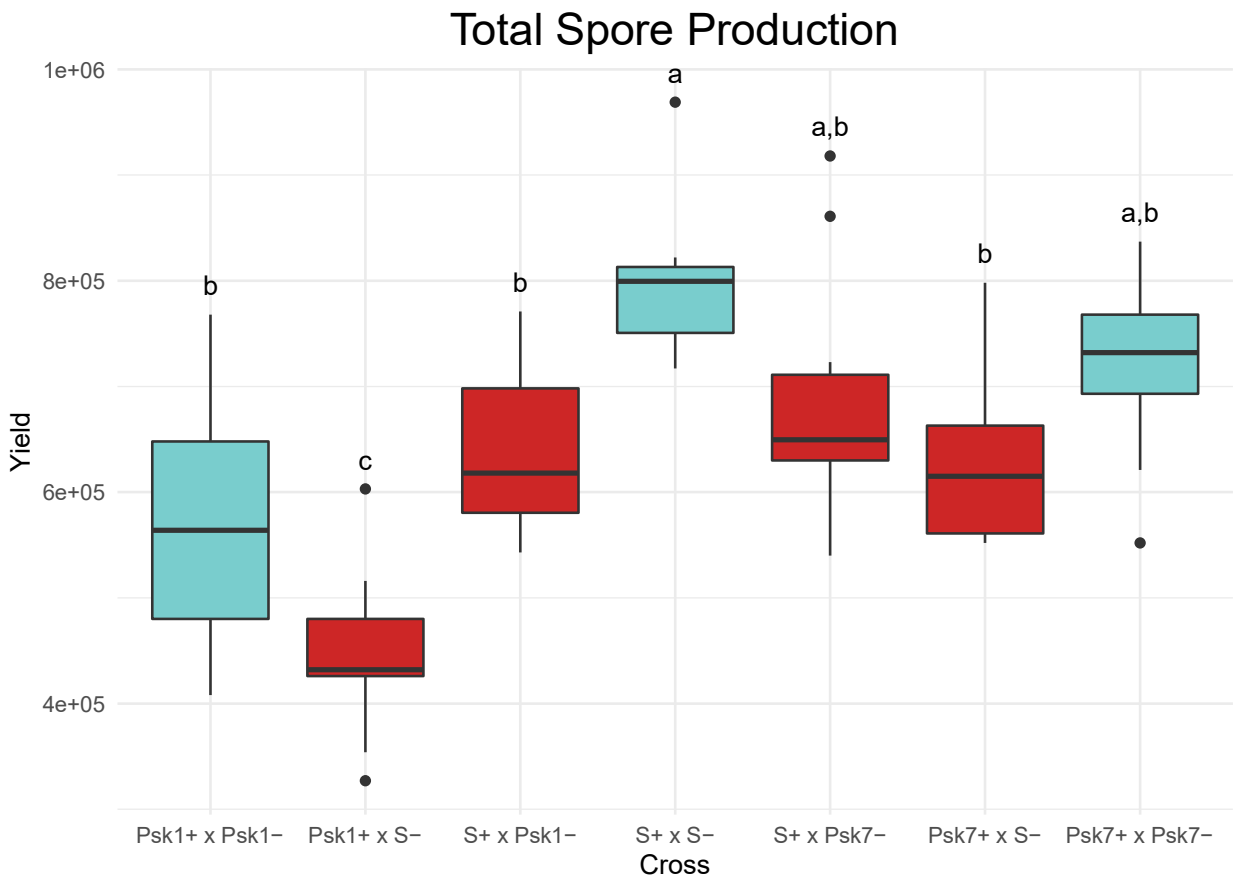

Figure 3. Plot showing the total amount of ascospores collected from crosses of isogenic strains possessing various iterations of the *Spok* block. Yield obtained in crosses where spore killing occurs are shown in blue; crosses with no spore killing are in red. Letters mark results of a Tukeys HSD test. The mating type is indicated by a + or – after the strain name. The *mat+* parent was always used as the maternal strain in crosses.

831 # Tables

832 **Table 1.** List of strains used in this study.

Strain	Species	*Psk*[a]	Genomic location	Size	*Enterprise*[b]	*Spok* genes
Wa21	*P. anserina*	2	Chr5 R	142433	*Spok* block	*Spok2 Spok3*
Wa28	*P. anserina*	2	Chr5 R	161297	*Spok* block	*Spok2 Spok3*
Wa46	*P. anserina*	naïve	-	-	absent	-
Wa53	*P. anserina*	1	Chr 3	113407	*Spok* block	*Spok2 Spok3 Spok4*
Wa58	*P. anserina*	7	Chr 5 L	167459	*Spok* block	*Spok2 Spok3 Spok4*
Wa63	*P. anserina*	S	-	-	absent	*Spok2*
Wa87	*P. anserina*	1	Chr 3	113425	*Spok* block	*Spok2 Spok3 Spok4*
Wa100	*P. anserina*	8	Chr 5 L	127869	*Spok* block	*Spok2 Spok4*
Wa137	*P. anserina*	9	Chr 1	247510	*Spok* block	*Spok2 Spok4*
S	*P. anserina*	S	-	-	absent	*Spok2*
Psk1xS_{14}[c]	*P. anserina*	1	Chr 3	113407	*Spok* block	*Spok2 Spok3 Spok4*
Psk7xS_{14}[c]	*P. anserina*	7	Chr 5 L	167459	*Spok* block	*Spok2 Spok3 Spok4*
T_G	*P. anserina*	5	Chr 3	157028	*Spok* block	*Spok3 Spok4*
Y	*P. anserina*	5	Chr 3	113435	*Spok* block	*Spok3 Spok4*
Wa131	*P. comata*	C1	-	-	absent	*Spok1*
Wa139	*P. comata*	C1	Chr5 L	38521	degraded	*Spok1*
T_D	*P. comata*	C1	-	-	absent	*Spok1*
CBS 237.71	*P. pauciseta*	P1	Chr 4	74163	*Spok* block	*Spok3 Spok4*

[a]Notice that a given *Spok* block might have *Spok3*, *Spok4* or both, and this reflects the *Psk* designation.
[b]The location of the *Spok* block and *Enterprise* element of Wa139 are indicated in the "Genomic Location" column. *Spok1* and *Spok2* are not found within the *Spok* block.
[c] Lab strains created by 14 consecutive backcrosses of *Psk-1* or *Psk-7* strains to S. The size of the *Spok* block is assumed to match that of the parental strain.

833

Supplementary Figures

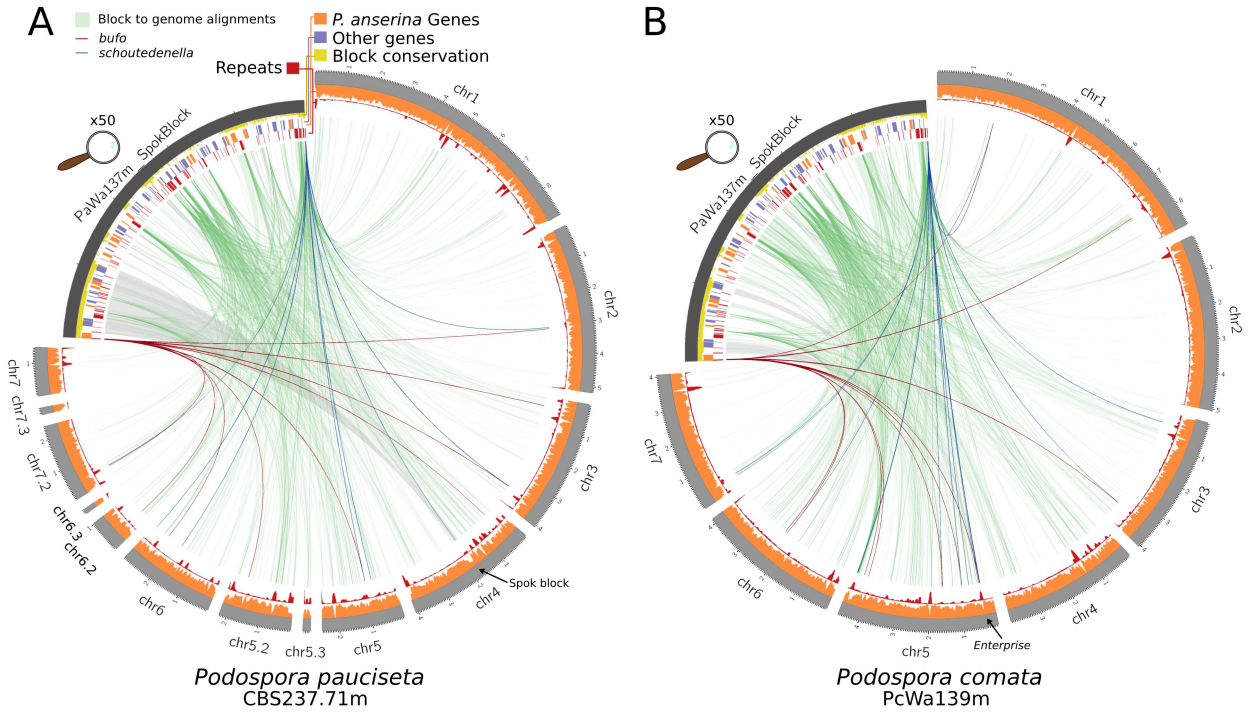

Supplementary Figure 1. Circos plots comparing the Wa137 *Spok* block to the genome of **A** the *P. pauciseta* strain CBS237.71 and **B** the *P. comata* strain Wa139.

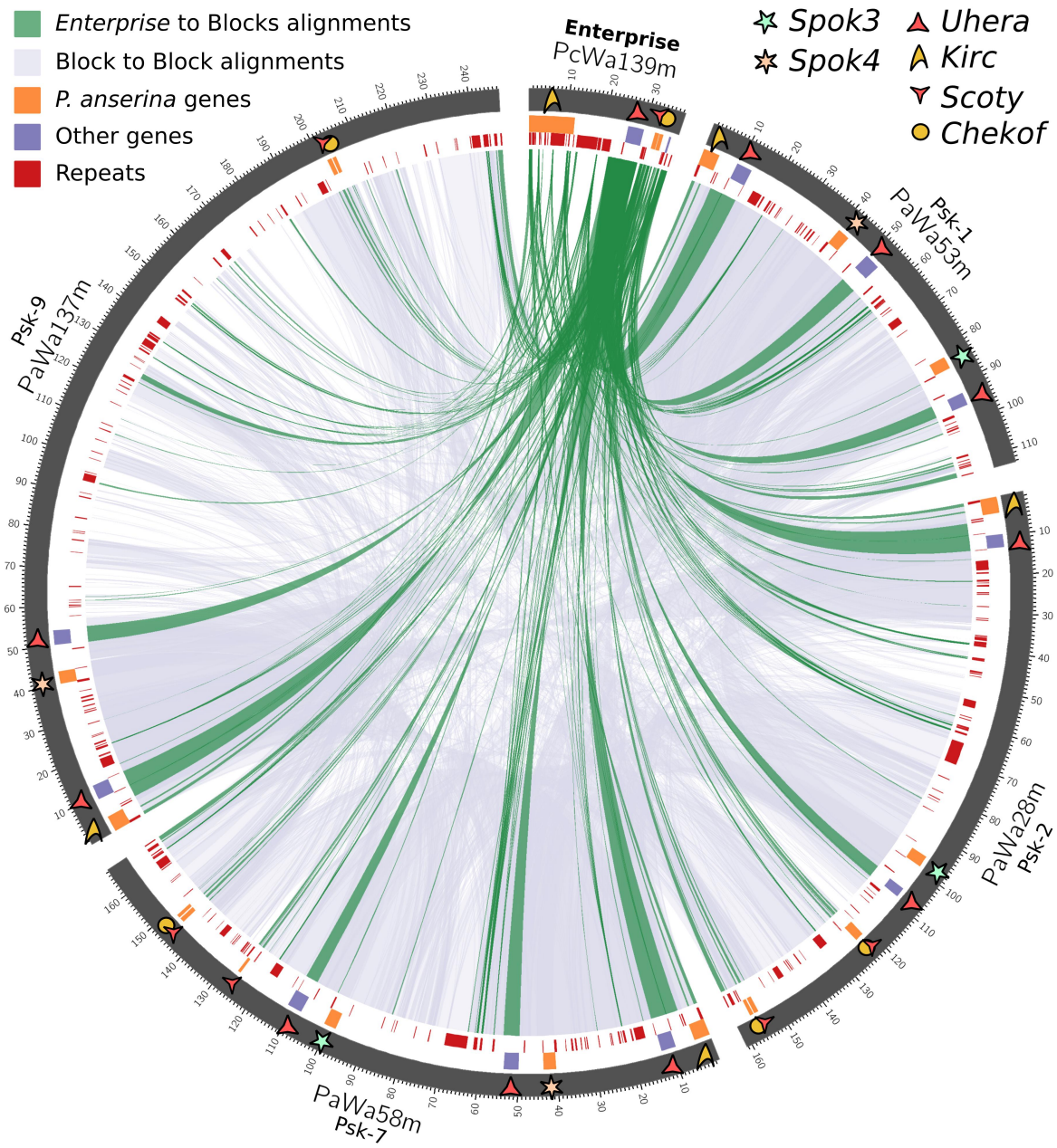

Supplementary Figure 2. A circos plot comparing the *Enterprise* of five different strains. Four of these represent different *Spok* blocks. Dark green lines connect homologous segments of the Wa139 *Enterprise* to the various *Spok* blocks. Lilac lines show homologous regions among the *Spok* blocks. Genes of interest are marked with symbols (See Supplementary Table 3).

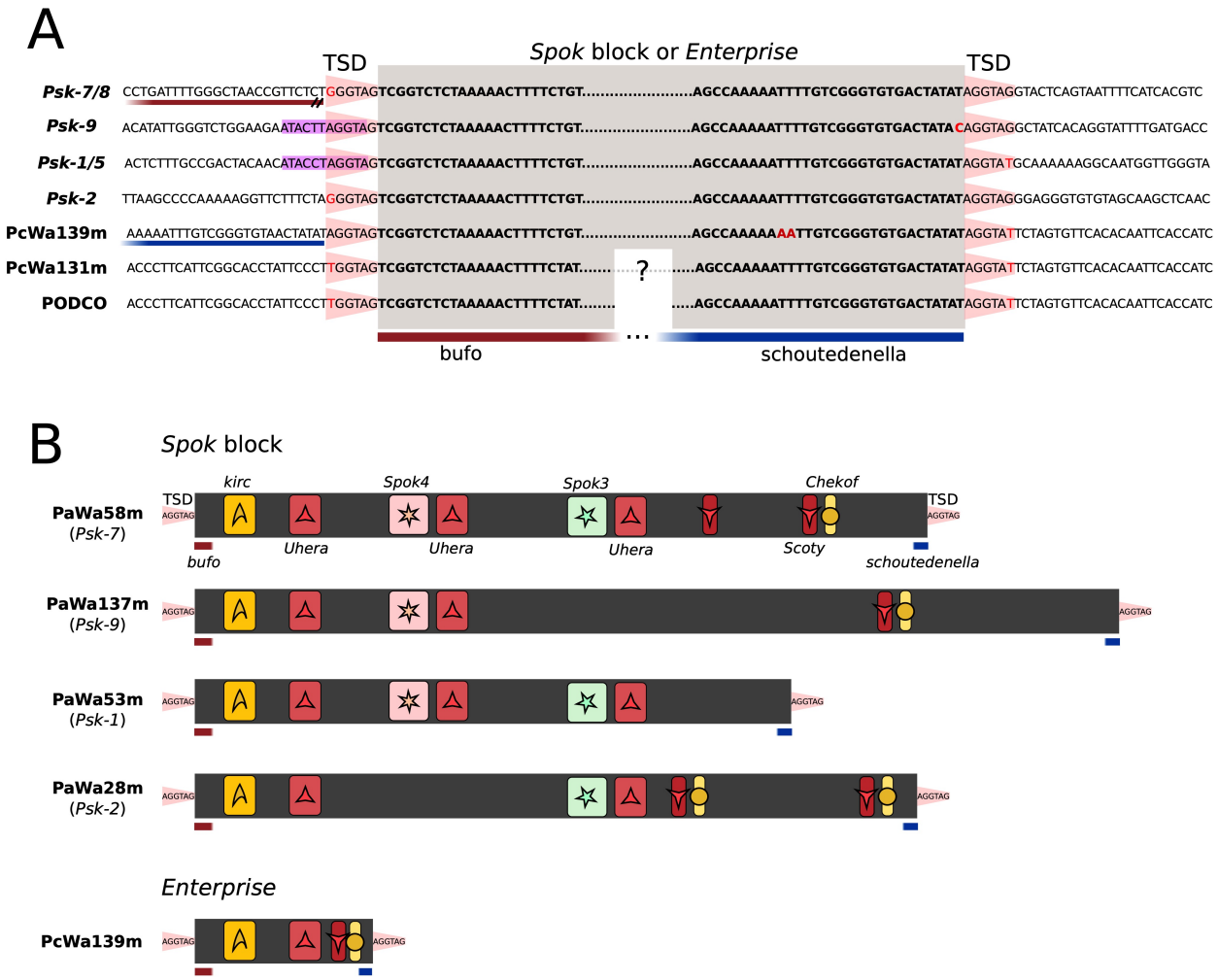

Supplementary Figure 3. Description of the *Spok* Block. **A** An alignment of the ends of four versions of the *Spok* block displaying the TSD (red trapezoid) plus the insertion site of *Enterprise* in three *P. comata* strains. The majority of *Enterprise* is deleted in the strain T_D (PODCO) and unassembled in Wa131. Additionally, Wa139 is inserted next to a copy of *schoutedenella* that is absent in both PODCO and Wa131. **B** Cartoon models representing the structure and gene content of four *Spok* blocks and of *Enterprise* from Wa139. Relevant genes and features are annotated. Not to scale.

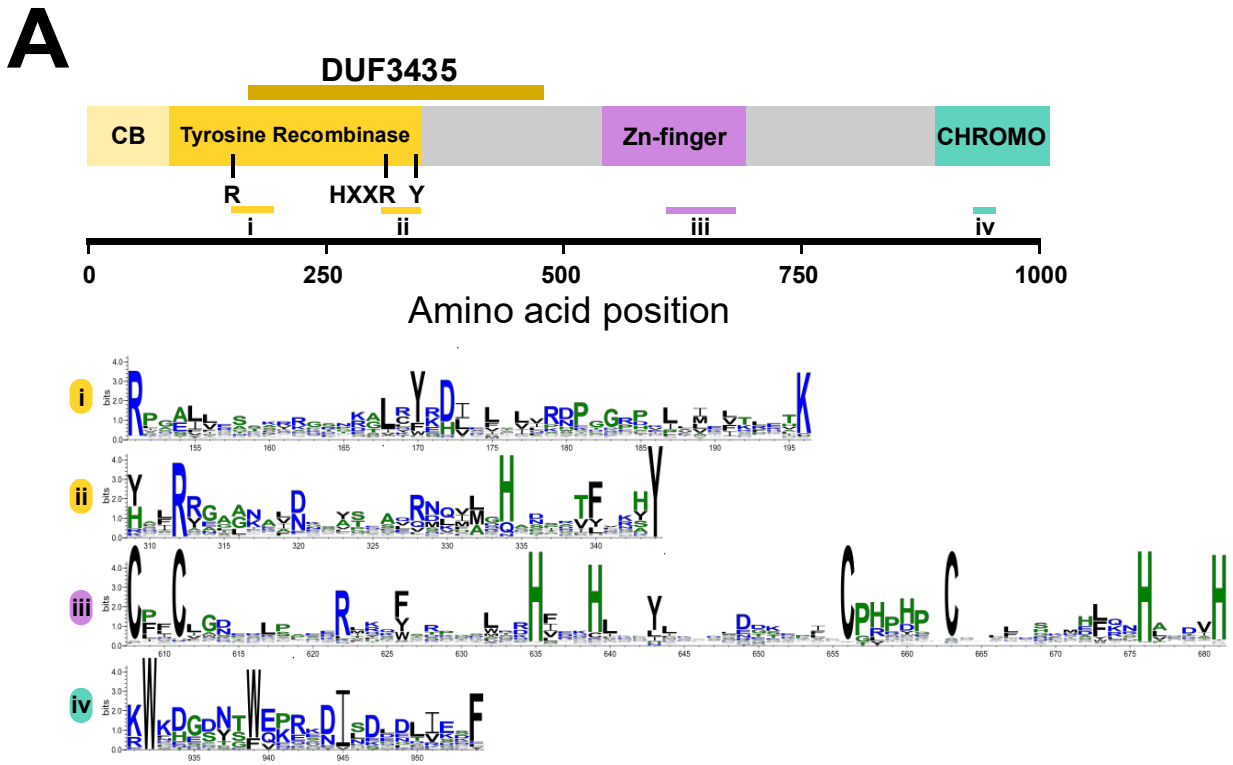

B

```
Kirc          HDFRAEGLYW-IDKLYSVAQRMKHAGQKDPNTYNNHY
Kirc_Msp      HDFRAEGLFW-IDKLYSVAQRMKYAGHKNSQMYNNHY
lambda        HELRSLSARL-YEKQISDKFAQHLLGHKSDTMAS-QY
Cre           HSARVGAARDMARAGVSIPEIMQAGGWTNVNIV-MNY
XerD          HVLRHAFATHLLNHGADLRVVQMLLGHSDLSTT-QIY
              *  *                                *
```

Supplementary Figure 4. Domain annotation of the *Kirc* protein obtained using HHPred. Four domains were identified: a N-terminal tyrosine recombinase domain with the associated core-binding domain, a central Zn-finger domain and a C-terminal chromodomain. An alignment of 279 *Kirc* homologs generated by Gremlin with HHBlits was used to create sequence logo of relevant regions of the *Kirc* sequences, including the active site regions of the tyrosine recombinase domain (i and ii), the Zn-finger region (iii) and the chromodomain region (iv) using Weblogo. **B**. Alignment of the *Kirc* sequence with an active site region of known tyrosine recombinases together with the sequence of a *Kirc* homolog from *Melanconium sp.*. Alignment is based on the HHPred output. Active site residues are marked with an asterisk. Kirc: *Kirc* gene in the *Spok* block of strain Wa58 (sites 309-344); Kirc_Msp: CE55503_10527 (110-145); lambda: lambda integrase PDB: 5J0N (308-342); Cre: recombinase enterobacteriaphage P1, PDB: 1XO0 (270-305); XerD: XerD site-specific recombinase E. coli, PDB: 1A0P (242-277).

Supplementary Figure 5. Alignment of four *Enterprise* elements within *Melanconnium sp.* revealing the TSD.

871 **Supplementary Table 1.** Assembly statistics for all strains with genomic data used in this study.

Species	Strain	Assembly	Technology	Assembler	Scaffolds[a]	N50	GC content	Size (bp)	Mean Depth long (x)
P. anserina	Wa21-	PaWa21m	PacBio	HGAP 3.0	9	5072363	51.49	35767411	80.3071
P. anserina	Wa28-	PaWa28m	PacBio	HGAP 3.0	7	5076631	51.41	35929333	76.2045
P. anserina	Wa46+	PaWa46p	PacBio	HGAP 3.0	9	4338573	51.37	35724019	117.8295
P. anserina	Wa53-	PaWa53m	PacBio	HGAP 3.0	7	4924837	51.52	35808992	83.821
P. anserina	Wa58-	PaWa58m	PacBio	HGAP 3.0	7	5037662	51.46	35985748	112.1709
P. anserina	Wa63+	PaWa63p	PacBio	HGAP 3.0	7	4907271	51.36	36002190	111.2245
P. anserina	Wa87+	PaWa87p	PacBio	HGAP 3.0	9	4338609	51.44	35896992	105.8792
P. anserina	Wa100+	PaWa100p	PacBio	HGAP 3.0	7	5096663	51.5	35953417	114.091
P. anserina	Wa137-	PaWa137m	MinION	Miniasm 0.2	9	4341106	51.08	36531367	49.924
P. anserina	Y+	PaYp	MinION	Miniasm 0.2	8	4821330	51.55	35719817	35.6112
P. anserina	T_G+	PaTgp	MinION	Miniasm 0.2	13	4230402	51.54	35778794	37.6743
P. pauciseta	CBS237.71-	CBS237.71m	MinION	Miniasm 0.2	13	4070182	51.6	35576233	24.3067
P. comata	Wa131-	PcWa131m	Illumina HiSeq	SPAdes 3.12.0	1119	258199	52.1	34680523	-
P. comata	Wa139-	PcWa139m	MinION	Miniasm 0.2	7	4603841	51.98	34819024	52.5779
P. anserina	**S+**	**Podan2**	**WGS**	**Arachne**	**7**	**4734292**	**52.17**	**35010595**	**-**
P. comata	**T_D+**	**PODCO**	**454 + Illumina**	**Newbler 2.3**	**7**	**4662433**	**52.42**	**34385490**	**-**

[a]The number of scaffolds correspond to those that map to the 7 chromosomes (excluding mitochondrial and rDNA contigs), but other columns include all scaffolds

[b]Numbers correspond to long-read data when available, otherwise to short-read data. For Wa139- and Wa137- the reads were filteread for QV>9 and to be larger than 1kb, resulting in 184301 and 202279 reads, respectively.

[c]Scaffolds larger than 50kb, excluding the mitochondrial and rDNA scaffolds

Species	Strain	Assembly	Mean Depth short (x)	No. Reads[b]	Mean Read Length (bp)	Repeat Content (%)[c]	Source
P. anserina	Wa21-	PaWa21m	78.0394	313285	11863	5.893	Vogan et al. 2019
P. anserina	Wa28-	PaWa28m	81.0651	327199	10105	5.961	Vogan et al. 2019
P. anserina	Wa46+	PaWa46p	107.4690	363721	12949	6.042	Vogan et al. 2019
P. anserina	Wa53-	PaWa53m	78.7383	327523	11382	5.924	Vogan et al. 2019
P. anserina	Wa58-	PaWa58m	88.3996	354055	13130	6.109	Vogan et al. 2019
P. anserina	Wa63+	PaWa63p	77.4007	351077	12562	6.223	Vogan et al. 2019
P. anserina	Wa87+	PaWa87p	74.3914	356924	12928	6.171	Vogan et al. 2019
P. anserina	Wa100+	PaWa100p	80.9098	361645	12857	5.914	Vogan et al. 2019
P. anserina	Wa137-	PaWa137m	143.6921	330780	7913	6.047	This study
P. anserina	Y+	PaYp	83.7234	697535	1952	5.873	Vogan et al. 2019
P. anserina	T_G+	PaTgp	155.9337	1286164	1384	6.009	Vogan et al. 2019
P. pauciseta	CBS237.71-	CBS237.71m	105.7037	240014	6188	6.056	Vogan et al. 2019
P. comata	Wa131-	PcWa131m	162.0216	39127244	150	3.555	This study
P. comata	Wa139-	PcWa139m	150.9355	236001	5786	3.769	This study
P. anserina	**S+**	**Podan2**	10	-	-	4.629	Espagne et al. 2008
P. comata	**T_D+**	**PODCO**	22	-	-	3.054	Silar et al. 2018

872

873 **Supplementary Table 2.** Hypothetical genes from within the *Spok* block of Wa137. Pfam domains inferred from NCBI conserved
874 domain database. Putative functions inferred from BLASTp to other genes with functional annotations. Blank cells indicate either no
875 pfam hits, or genes with BLASTp results to only hypothetical genes.
876

Gene code|name in Wa137	**pfam**				**Putative function**
gene01805|Kirc	DUF3435 superfamily	CD_CSD superfamily	CHROMO		
gene01806|Uhera1	DEAD-like_ helicase_C superfamily	DEAD-like_helicase_N superfamily			
PaWa137m.02400|PpBr36_10652_ Pyricularia_pennisetigena	Peptidase_C48 superfamily				
PaWa137m.02401| Pa_2_5490_homolog	NAP				
PaWa137m.02402|S7711_11618_ Stachybotrys_chartarum_homolog					NAD-dependent protein deacetylase
PaWa137m_chromosome_1.2:hsp:12095 1:4.5.0.58|Pa_7_10380_fragment					
PaWa137m_CH35J_006576| CH35J_006576_Colletotrichum_ higginsianum_fragment	Patatin_and_cPLA2 superfamily				Phospholipase A2
PaWa137m.02404| PODCO_502086_Fragment	DDE_Tnp_ISL3 superfamily				PKS-NRPS hybrid synthetase
PaWa137m.02405| Pa_4_1058_homolog					
gene00315|Spok4					Spore killer
PaWa137m.Pa_5_2010_fragment1| Pa_5_2010_fragment1					GPI anchored serine-threonine rich protein
gene01852|Uhera2					
PaWa137m_Pa_1_14730_fragment1| Pa_1_14730_fragment					EST/SMG-like protein 1

gene01815|Pa_6_9560_Fragment	p450 superfamily				pisatin demethylase
gene01816|Pa_6_9560_homolog	p450 superfamily				pisatin demethylase
PaWa137m_7_6640_fragment| Pa_7_6640_Fragment	Peptidase_M16_M superfamily				insulysin
PaWa137m_CTA1_5148| PaWa137m_CTA1_5148_ Colletotrichum_tanaceti_fragment	NK superfamily				Uridylate kinase
PaWa137m.gene.002245| Pa_6_9580_homolog					Satratoxin biosynthesis SC1 cluster protein 4
gene01818|Pa_4_3510_homolog	Peptidase_C48 superfamily	GumC superfamily			
PaWa137m.gene.002249| Pa_1_13070_fragment	zf-H2C2_2	zf-C2H2	COG5048		cutinase G-box binding protein
PaWa137m.gene.PODCO_102140| PODCO_102140_fragment	ABC_ATPase superfamily				Heavy metal tolerance protein
gene01820|PV05_03319_ Exophiala_xenobiotica_fragment	MdlB				Heavy metal tolerance protein
PaWa137m.02410| Pa_6_7965_homolog					
gene01823|Pa_1_13070_homolog	zf-C2H2	zf-H2C2_2	zf-C2H2	lambda-1 superfamily	cutinase G-box binding protein
PaWa137m_Pa_6_2490_fragment| Pa_6_2490_fragment					
gene01824| PODCO_511675_homolog					
PaWa137m_Pa_6_2440_fragment| Pa_6_2440_fragment	PRK09605 superfamily				
PaWa137m_MBR_09427_ Metarhizium_brunneum_fragment| PaWa137m_MBR_09427_ Metarhizium_brunneum_fragment					mitofusin
gene01824.2| PODCO_511675_homolog_2					

PaWa137m_Pa_1_14730_fragment					EST/SMG-like protein 1
PaWa137m.02414|S40285_10826_ Stachybotrys_chlorohalonata_ homolog					
PaWa137m.02415| Micbo1qcDRAFT_170078_ Microdochium_bolleyi_homolog					
PaWa137m.02416| Pa_5_2010_homolog					GPI anchored serine-threonine rich protein
PaWa137m.gene.002259| Pa_6_8910_homolog	AdoMet_MTases superfamily				Trans-aconitate 2-methyltransferase
gene01828|CHGG_04275_ Chaetomium_globosum					
gene01830|DL98DRAFT_554023_ Cadophora_sp_homolog					
gene01831|MBR_09427_ Metarhizium_brunneum_homolog					mitofusin
WaPa137m_4_1930| Pa_4_1930_fragment	Isoprenoid_Biosyn _C1 superfamily				Iridoid synthase
PaWa137m.gene.002264| CHGG_09441_ Chaetomium_globosum_homolog					
PaWa137m_NA56DRAFT_749014_ Pezoloma_ericae_fragment| PaWa137m_NA56DRAFT_749014_ Pezoloma_ericae_fragment					
PaWa137m.gene.002265|PV05_03319_ Exophiala_xenobiotica_fragment	ABC_ATPase superfamily				ABC transporter
gene01834|SPI_07993_homolog_ Metallophosphoesterase	MPP_Dcr2				Metallo-dependent phosphatase
PaWa137m_K432DRAFT_223816_ Lepidopterella_palustris_homolog| PaWa137m_K432DRAFT_223816_ Lepidopterella_palustris_homolog	TPR_12				

gene01835|Pa_1_1830_homolog	GT2_HAS				Hyaluronan synthase
gene01836|Pa_1_14730_homolog	EST1_DNA_bind superfamily				EST/SMG-like protein 1
PaWa137m.02425|S7711_10142_ Stachybotrys_chartarum_homolog	CD_CSD superfamily				
PaWa137m_HIM_12183|HIM_12183_ Hirsutella_minnesotensis_homolog	Pkinase superfamily				
PaWa137m_M441DRAFT_90628| M441DRAFT_90628_ Trichoderma_asperellum_homolog					
gene01838|S7711_11475_ Stachybotrys_chartarum_homolog					
gene01839|S40293_11413_ Stachybotrys_chartarum					patatin-like serine hydrolase
gene01840|NA56DRAFT_703776_ Pezoloma_ericae_homolog	DUF3723 superfamily	PTZ00121 superfamily			
gene01841|Micbo1qcDRAFT_129033_ Microdochium_bolleyi_homolog					Satratoxin biosynthesis SC1 cluster protein 4
gene01842|Pa_5_3190_homolog	MFS superfamily				Efflux pump FUS6
gene01843|Pa_7_6640_homolog	Ptr superfamily				insulysin
PaWa137m_SS1G_08066_Sclerotinia_ sclerotiorum_homolog|Scoty					
gene01844|Chekof	PKc_like superfamily				
PaWa137m_Pa_1_1830_fragment	Peptidase_C48 superfamily				
PaWa137m.gene.002278|PpBr36_10652 _ Pyricularia_pennisetigena_homolog					
gene01845|Pa_4_3510_fragment					
gene01847|GE09DRAFT_1263105_ Coniochaeta_sp_homolog	MdlB				Heavy metal tolerance protein

gene01849|CHGG_09572_ Chaetomium_globosum_fragment					Putative AC transposase
gene01850|MBR_09427_ Metarhizium_brunneum_homolog					
PaWa137m_AJ78_06594_ Emergomyces_pasteurianus_ homolog| PaWa137m_AJ78_06594_ Emergomyces_pasteurianus_ homolog					
PaWa137m.02432| Pa_5_3190_homolog	MFS superfamily				Efflux pump FUS6
PaWa137m_CSUB01_08519_ Colletotrichum_sublineola_homolog	CFEM superfamily				Satratoxin biosynthesis SC1 cluster protein 4
PaWa137m.gene.002286| MYCTH_64320_ Thermothelomyces_thermophilus_ homolog					
PaWa137m_DL765_007700_ Monosporascus_sp_fragment| PaWa137m_DL765_007700_ Monosporascus_sp_fragment					

877